

High Efficiency Desulfurization of Synthesis Gas

Annual Report

September 2002 – August 2003

Kwang-Bok Yi
Elizabeth J. Podlaha
Douglas P. Harrison

November 2003

DE-FG26-00NT40813

Gordon A. and Mary Cain Department of Chemical Engineering
Louisiana State University
Baton Rouge, LA 70803

DISCLAIMER

This report was prepared as an account of work sponsored by an agency of the United States Government. Neither the United States Government nor any agency thereof, nor any of their employees, makes any warranty, express or implied, or assumes any legal liability or responsibility for the accuracy, completeness, or usefulness of any information, apparatus, product, or process disclosed, or represents that its use would not infringe privately owned rights. Reference herein to any specific commercial product, process, or service by trade name, trademark, manufacturer, or otherwise does not necessarily constitute or imply its endorsement, recommendation, or favoring by the United States Government or any agency thereof. The views and opinions of authors expressed herein do not necessarily state or reflect those of the United States Government or any agency thereof.

ABSTRACT

Mixed metal oxides containing CeO_2 and ZrO_2 are being studied as high temperature desulfurization sorbents capable of achieving the DOE Vision 21 target of 1 ppmv or less H_2S . The research is justified by recent results in this laboratory that showed that reduced CeO_2 , designated CeO_n ($1.5 < n < 2.0$), is capable of achieving the 1 ppmv target in highly reducing gas atmospheres. The addition of ZrO_2 has improved the performance of oxidation catalysts and three-way automotive catalysts containing CeO_2 , and should have similar beneficial effects on CeO_2 desulfurization sorbents.

An electrochemical method for synthesizing $\text{CeO}_2\text{-ZrO}_2$ was developed and the products were characterized by XRD and TEM during year 01. Nanocrystalline particles having a diameter of about 5 nm and containing from approximately 10 mol% to 80 mol% ZrO_2 were prepared. XRD analysis showed the product to be a solid solution at low ZrO_2 contents with a separate ZrO_2 phase emerging at higher ZrO_2 levels. Unfortunately, the quantity of $\text{CeO}_2\text{-ZrO}_2$ that could be prepared electrochemically was too small to permit full desulfurization testing.

Also during year 01 a laboratory-scale fixed-bed reactor was constructed for desulfurization testing. All components of the reactor and analytical systems that may be exposed to low concentrations of H_2S are constructed of quartz, Teflon, or silcosteel. Reactor product gas composition as a function of time is determined using a Varian 3800 gas chromatograph equipped with a pulsed flame photometric detector (PFPD) for measuring low H_2S concentrations ($< \sim 10$ ppmv) and a thermal conductivity detector (TCD) for higher concentrations of H_2S .

Larger quantities of $\text{CeO}_2\text{-ZrO}_2$ mixtures from other sources, including mixtures prepared in this laboratory using a coprecipitation procedure, have been obtained. Much of the work during year 02 consisted of characterization and desulfurization testing of materials obtained from commercial sources. To properly evaluate the effect of ZrO_2 addition on desulfurization capability, the physical properties of the sorbent must be similar. That is, a $\text{CeO}_2\text{-ZrO}_2$ mixture from source A would not necessarily be superior to pure CeO_2 from source B if the properties were dissimilar. Therefore, research during year 03 concentrated CeO_2 and $\text{CeO}_2\text{-ZrO}_2$ mixtures prepared in this laboratory using the coprecipitation procedure. The structure of these sorbents is similar and the effect of ZrO_2 addition can better be separated from other effects.

X-ray diffraction tests of the sorbents prepared in house have confirmed the existence of a solid solution of ZrO_2 in CeO_2 . Reduction tests using an electrobalance reactor have confirmed that $\text{CeO}_2\text{-ZrO}_2$ mixtures are more easily reduced than pure CeO_2 . Reduction of $\text{CeO}_2\text{-ZrO}_2$ begins at a lower temperature and the final value of n in CeO_n ($1.5 < n < 2.0$) is smaller in $\text{CeO}_2\text{-ZrO}_2$ than in pure CeO_2 . Desulfurization tests have shown that both CeO_2 and $\text{CeO}_2\text{-ZrO}_2$ sorbents are capable of reaching the target sub-ppmv H_2S level in highly reducing gases. Both CeO_2 and $\text{CeO}_2\text{-ZrO}_2$ sorbents have successfully removed H_2S to the minimum detectable limit of the PFPD detector, approximately 100 ppbv.

TABLE OF CONTENTS

Disclaimer	ii
Abstract	iii
Table of Contents	iv
List of Figures	v
List of Tables	vi
Executive Summary	vii
 1. INTRODUCTION	 1
1.1. High Temperature Gas Desulfurization	1
1.2 Ceria-Zirconia Catalyst Research	3
1.3 Objectives of the Research.....	3
2. ELECTROCHEMICAL SYNTHESIS AND CHARACTERIZATION OF CeO ₂ -ZrO ₂	4
2.1. Electrochemical Experimental	4
2.2. Solid State Analyses	4
2.2.1. Composition	6
2.2.2. XRD and TEM Characterization	6
3. HIGH TEMPERATURE DESULFURIZATION TEST EQUIPMENT.....	9
3.1. Fixed-Bed Reactor	9
3.2. Gas Analysis	11
4. SORBENT MATERIALS	14
4.1. Commercial Sorbents	14
4.2 LSU Sorbents	17
5. SORBENT REDUCTION.....	20
5.1. Commercial Sorbents.....	20
5.2. LSU Sorbents.....	21
6. FIXED-BED DESULFURIZATION RESULTS.....	22
6.1. Commercial Sorbents.....	26
6.2 LSU Sorbents.....	28
7. CONCLUSIONS	32
8. REFERENCES	34

LIST OF FIGURES

Figure 1. Electrochemical Cell Schematic	5
Figure 2. Electrolyte Concentration vs. Final Powder Concentration	6
Figure 3. TEM Images of (a) Ceria, (b) Ceria-7 at.% Zirconia (C) Ceria-18 at.% Zirconia	7
Figure 4. XRD Analysis of (a) Electrochemically Generated Nanocrystalline $\text{Ce}_{0.82}\text{Zr}_{0.18}\text{O}_2$, (b) Cubic CeO_2 (JCPDS 34-394), and (c) Monoclinic (JCPDS 37-1484) and Tetragonal (JCPDS 42-1164) ZrO_2	8
Figure 5. Heat Treated 700°C, 18.7 mol % Zr Ceria-Zirconia with Resulting Crystallite Size of (a) 9.5 nm, (b) 10 nm, (c) 11 nm, (d) 12 nm, (e) 12.5 nm, (f) 12.5 nm, and (g) 14.5 nm	9
Figure 6. Fixed-Bed Reactor System	10
Figure 7. Details of the Quartz Reactor	11
Figure 8. Chromatograph Sampling Arrangement	13
Figure 9. PFPD Calibration Curve	15
Figure 10. PFPD Chromatogram at 0.01 ppmv H_2S	15
Figure 11. TCD Calibration Curve	16
Figure 12. XRD Spectrum of CZ(Nex)80.....	17
Figure 13. XRD Spectra of CZ(LSU)80 and Ce(LSU)	18
Figure 14. Equilibrium Oxygen Pressure in Reducing Gases 2 and 3	19
Figure 15. Reduction of Ce(RP).....	20
Figure 16. Comparison of the Reducibility of Ce(RP) and CZ(Nex)80 in Reducing Gas 1	21
Figure 17. Comparison of Reducibility of Ce(LSU) and CZ(LSU) Sorbents in Gas 3	23
Figure 18. Typical Sulfidation Breakthrough Curves and Sorbent Conversions for Duplicate Tests (Full Concentration Scale).....	24
Figure 19. Typical Sulfidation Prebreakthrough Curves for Duplicate Tests (Expanded Concentration Scale).....	25
Figure 20. Prebreakthrough Sulfidation Results from Three Commercial CeO_2 Sorbents.....	26
Figure 21. The Effect of Temperature on the Sulfidation of Ce(RP)	27
Figure 22. Comparison of the Sulfidation Performance of Ce(RP) and CZ(Nex)...	28
Figure 23. Comparison of the Sulfidation Performance of Ce(LSU), CZ(LSU)90, and CZ(LSU)80	29
Figure 24. The Effect of Pre-Reduction on Sulfidation of CZ(LSU)80.....	30
Figure 25. The Effect of Temperature on Sulfidation of CZ(LSU)80.....	30
Figure 26. The Effect of CO_2 in the Sulfidation Gas on Performance of Ce(LSU) (Full Concentration Scale).....	31
Figure 27. The Effect of CO_2 in the Sulfidation Gas on Performance of Ce(LSU) (Expanded Concentration Scale).....	31
Figure 28. The Effect of CO_2 in the Sulfidation Gas on Performance of CZ(LSU)80 (Full Concentration Scale).....	32
Figure 29. The Effect of CO_2 in the Sulfidation gas on Performance of CZ(LSU)80 (Expanded Concentration Scale).....	33

LIST OF TABLES

Table 1. Composition of the Various Electrolyte Solutions	5
Table 2. Gas Chromatograph Operating Conditions	12
Table 3. Commercial CeO ₂ and CeO ₂ -ZrO ₂ Materials with Selected Properties....	16
Table 4. CeO ₂ and CeO ₂ -ZrO ₂ Materials Prepared at LSU by Coprecipitation ...	18
Table 5. Summary of Reduction Results from Commercial Sorbents.....	22
Table 6. Summary of Reduction Results from LSU Sorbents.....	23
Table 7. The Relation Between Dimensional Time and Dimensionless Time = 1..	25

EXECUTIVE SUMMARY

The DOE Vision 21 program requires more stringent control of H₂S concentration in coal-derived synthesis gas to be used in certain applications. Previous target levels of about 20 ppmv H₂S suitable for electric power generation using an integrated gasification combined cycle process (IGCC) have been replaced by H₂S targets of 1 ppmv or less required for fuel cell and other catalytic processes.

Zinc-based sorbents developed for IGCC applications are not capable of achieving the Vision 21 target at high temperatures. Reduced cerium oxide, CeO_n (1.5 < n < 2.0), has recently been shown to be capable of reducing H₂S to less than 1 ppmv at temperatures near 700°C in gas atmospheres having greater reducing power than typical coal-derived gases. Related research in oxidation catalysis and three-way automotive catalysis has shown that catalyst performance is improved by the addition of ZrO₂ to the CeO₂. The reasons given for the improved performance, including increased oxygen exchange capacity, should also result in improved desulfurization performance.

This research project consists of two major activities – the electrochemical synthesis and characterization of CeO₂-ZrO₂ materials, and high temperature desulfurization tests using CeO₂-ZrO₂ sorbents. Electrochemical synthesis was the primary focus during year 01 and results were presented in the first annual report (Mukherjee et al. 2001). Nanocrystalline powders of approximately 5 nm diameter and containing from 10 mol% to 80 mol% ZrO₂ were deposited at an electrode surface using the cathodic generation of base method. Conditions required for the production of desired solid solutions of CeO₂-ZrO₂ having a fluorite-type structure were identified. A separate ZrO₂ phase was formed at high ZrO₂ concentration. Heat treatment at 700°C for as long as 106 hrs at 700°C produced no phase separation, but the crystallite size increased from 5 nm to 14.5 nm. Unfortunately, the quantities of CeO₂-ZrO₂ that could be produced using this method were too small to permit realistic desulfurization testing, and other sources of CeO₂-ZrO₂ sorbents were pursued. A summary of that work is repeated in this report.

A laboratory-scale fixed-bed reactor having a capacity of about 15 g of solid was constructed during year 01 for desulfurization testing. In order to avoid interaction between low concentrations of H₂S and stainless steel, all components of the reactor and analytical systems that may be exposed to low H₂S concentrations were constructed of quartz, Teflon, or silcosteel. Reactor product gas composition as a function time is determined using a Varian 3800 gas chromatograph purchased for this project with LSU matching funds. The chromatograph is equipped with a pulsed flame photometric detector (PFPD) for measuring low H₂S concentrations (< ≈10 ppmv) and a thermal conductivity detector (TCD) for higher concentrations of H₂S.

Larger quantities of CeO₂ and CeO₂-ZrO₂ suitable for desulfurization testing were obtained from a number of commercial sources. Characterization and desulfurization testing of these sorbents was emphasized during year 02. X-ray diffraction tests confirmed the existence of a solid solution of ZrO₂ in CeO₂. Reduction tests using an

electrobalance reactor confirmed that $\text{CeO}_2\text{-ZrO}_2$ mixtures are more easily reduced than pure CeO_2 . Reduction began at a lower temperature and the final value of n in CeO_n ($1.5 < n < 2.0$) was smaller in $\text{CeO}_2\text{-ZrO}_2$ than in pure CeO_2 .

Desulfurization tests using commercial sorbents from different sources, prepared by different methods and having different properties, proved that to evaluate the effect of ZrO_2 addition, the sorbents must have similar physical properties. That is, a $\text{CeO}_2\text{-ZrO}_2$ mixture from one source would not necessarily have superior desulfurization ability than pure CeO_2 from another source unless the two sorbents had similar physical properties. Experimental results using these commercial sorbents were described in annual report 02 (Yi et al. 2002) and are summarized in this report.

This report emphasizes the preparation, characterization, and desulfurization testing of CeO_2 and $\text{CeO}_2\text{-ZrO}_2$ sorbents prepared in this laboratory using a co-precipitation technique. The structure of these sorbents is similar allowing the effect of ZrO_2 addition to be better understood. The LSU sorbents containing as much as 20 mol% ZrO_2 also formed solid solutions in CeO_2 . ZrO_2 -containing materials were more easily reduced than ZrO_2 -free sorbents. However, the degree of reduction of the LSU $\text{CeO}_2\text{-ZrO}_2$ sorbents was somewhat less than obtained from commercial $\text{CeO}_2\text{-ZrO}_2$ sorbents obtained from NexTech Co. The differences in degree of reduction are attributed to different structural characteristics of the two materials.

Desulfurization tests using the LSU sorbents have been limited to 1 bar because of the quartz reactor and have examined the effects of temperature, pre-reduction in a sulfur-free gas, and sulfidation gas composition. Pre-breakthrough H_2S concentrations below the 1 ppmv target have been obtained consistently in highly reducing gases using both CeO_2 and $\text{CeO}_2\text{-ZrO}_2$ sorbents. CO_2 was added as a source of oxygen to control the reducing power of the feed gas. As the CO_2 concentration increased the desulfurization performance of all sorbents suffered. Sub-ppmv H_2S concentrations were achieved during the prebreakthrough period, but the duration of the prebreakthrough period decreased as the CO_2 concentration increased.

I. INTRODUCTION

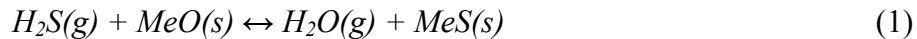
Research relating to the high temperature desulfurization of coal-derived gas has been a major component of the DOE fossil energy program for a number of years. In the past, the primary objective was to reduce H_2S concentration to levels required for electric power generation using integrated gasification combined cycles (IGCC), approximately 20 ppmv. Desulfurization processes for this application using zinc-based sorbents have progressed to the demonstration stage. The new DOE Vision 21 program, however, requires much more stringent sulfur control measures. Sulfur levels equal to or less than 1 ppmv are required for fuel cells and certain synthesis gas catalytic processes. New sorbents are needed to meet these more stringent sulfur limits.

Recent research in this laboratory (Zeng et al. 1999, Zeng et al. 2000) showed that reduced cerium oxide, designated CeO_n ($1.5 < n < 2.0$), is capable of reducing H_2S from 1 mol% to less than 1 ppmv at temperatures near $700^\circ C$ in highly reducing gas compositions. However, the product compositions from gasifiers currently available in the United States (Texaco, KRW, etc.) do not have the reducing power required to achieve significant CeO_2 reduction. The equilibrium H_2S content in contact with unreduced CeO_2 is well above the more stringent Vision 21 target levels.

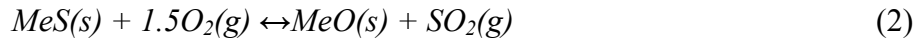
This research is continuing the investigation of CeO_2 sorbents and extending the investigation to the performance of mixed oxide sorbents of CeO_2 - ZrO_2 with the objective of meeting Vision 21 target levels in less reducing gas compositions. The addition of ZrO_2 to CeO_2 has improved the performance of oxidation catalysts and three-way automotive catalysts. The improvement is attributed to increased reducibility and improved oxygen mobility resulting from the addition of ZrO_2 , factors that should also improve desulfurization performance.

1.1. High Temperature Gas Desulfurization

High temperature desulfurization of coal-derived gas is based on the noncatalytic gas-solid reaction between H_2S and an appropriate metal oxide. The reaction may be written generically as follows:



The generic reaction for the regeneration of the metal sulfide is:

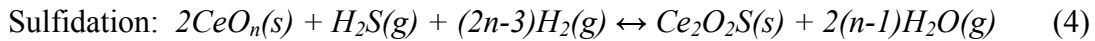
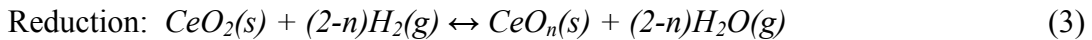


For economic reasons, the sorbent must maintain activity through many sulfidation-regeneration cycles. A number of metals including Zn, Fe, Mn, Cu, and Ca have been studied but most of the recent research has focused on Zn-based materials, including ZnO (e.g., Gibson and Harrison 1980), $ZnFe_2O_4$ (e.g., Focht et al. 1988), and $ZnO \cdot xTiO_2$ (e.g., Woods et al. 1990).

Harrison (1998) has discussed the advantages and disadvantages of zinc-based sorbents. Advantages include favorable desulfurization thermodynamics, rapid kinetics, large stoichiometric sulfur capacity (39 g S/100 g ZnO), and relatively low cost. Disadvantages include the tendency for ZnO to be reduced to volatile metallic Zn at high temperature, the highly exothermic nature of the regeneration reaction, and the possible formation of ZnSO₄ during regeneration. The tendency for ZnO reduction followed by Zn vaporization can be moderated, but not eliminated, by the addition of TiO₂ to form the mixed metal oxide ZnO•xTiO₂. However, TiO₂ addition increases the sorbent processing cost and reduces the sulfur capacity. Dilute O₂ may be used to control temperature during regeneration, but this causes dilute SO₂ to be produced and complicates the ultimate sulfur control problem. ZnSO₄, because of its large molar volume, has been identified as a cause of rapid sorbent deterioration in multicycle tests, and careful control of temperature and the partial pressures of O₂ and SO₂ are required to prevent its formation.

The performance of CeO₂ as a high temperature desulfurization sorbent was recently studied in this laboratory (Zeng et al. 1999, Zeng et al. 2000). H₂S concentrations were reduced from 1 mol% (10,000 ppmv) to 1 ppmv or less at temperatures in the range of 650°C to 800°C in highly reducing atmospheres. Reduction of CeO₂ to oxygen-deficient CeO_n (n < 2) was the key in achieving low H₂S concentrations. The sulfided product, Ce₂O₂S, was easily regenerated using SO₂ with sulfur liberated in elemental form. Preliminary multicycle tests (25 complete cycles) showed no evidence of sorbent deterioration.

The complete cycle using cerium sorbent consists of three steps – reduction, sulfidation, and regeneration – as shown by the following reactions.



Reactions (3) and (4) occur simultaneously in the reducing synthesis gas. The ultimate degree of reduction, i.e., the equilibrium value of n, depends on temperature and the oxygen partial pressure of the reducing gas, as described by Bevan and Kordis (1964) and Sorensen (1976). Reduction experiments in this laboratory using CeO₂ and an electrobalance reactor have shown that the level of reduction, i.e., the experimental value of n, is in reasonable agreement with the results of Bevan and Kordis. Unfortunately the oxygen partial pressure in the product gas from typical U.S coal gasifiers (Texaco and KRW) is too large to achieve significant CeO₂ reduction.

The current research is examining the addition of ZrO₂ to CeO₂ in the hope that reduction to CeO_n can be more easily accomplished. The expected benefits are based on results from recent research in the areas of oxidation and automotive catalysis summarized in the following section.

1.2. Ceria-Zirconia Catalyst Research

CeO₂ serves an important role in three-way automotive catalysts (TWC) by regulating the oxygen pressure in the exhaust gas. During fuel rich operation, CeO₂ is reduced to CeO_n and the oxygen released assists in the oxidation of CO and hydrocarbons to CO₂. Under fuel lean conditions CeO_n is re-oxidized to CeO₂ and removal of oxygen from the gas phase assists in the reduction of NO_x to N₂. In oxidation catalysis, the CeO₂ is reduced to CeO_n by surface adsorbed species as they are oxidized to CO₂, and the CeO_n is then re-oxidized to CeO₂ by oxygen from the gas phase.

Recent research has shown that the addition of ZrO₂ to CeO₂ enhances the redox reactions. Colon et al. (1998) state that the addition of ZrO₂ enhances the oxygen mobility within the crystal and improves the catalyst thermal stability at 1000°C. Zamar et al. (1995) discuss the enhanced oxygen storage and release capacity of CeO₂-ZrO₂ mixtures used for CH₄ combustion. ZrO₂ was said to promote the formation of oxygen vacancies and increase the mobility of bulk oxygen. The 50% CH₄ conversion level was reached at a temperature 130°C lower using Ce_{0.8}Zr_{0.2}O₂ compared to CeO₂ alone.

Hori et al. (1998) report an increase in reversibly stored oxygen by a factor of 1.7-2.5 for phase separated CeO₂-ZrO₂ compared to CeO₂ alone, and by a factor of 3 to 5 for solid solutions of CeO₂-ZrO₂. The optimum Zr concentration was 25 mol%, but performance was relatively insensitive to Zr loading between 15 mol% and 50 mol%. Bunluesin et al. (1997) found that addition of ZrO₂ slowed the catalyst deactivation rate for CO oxidation over a Ce-Pd catalyst. Deactivation without ZrO₂ was attributed to a large increase in crystallite size, and ZrO₂ was said to slow crystallite growth.

Trovarelli et al. (1997) and Cuif et al. (1996) discuss the improved performance of three-way automotive catalysts due to the addition of ZrO₂ to CeO₂. Trovarelli et al. state that the addition of ZrO₂ enhances the catalytic, textural, redox, and oxygen storage properties of ceria. Trovarelli (1996) and Ozawa (1997) have published recent reviews describing the beneficial effects of ZrO₂ addition.

These positive effects on the performance of CeO₂ catalysts associated with ZrO₂ addition – improved redox potential, increased oxygen mobility, higher oxygen exchange capacity, improved activity at lower temperature, and increased thermal stability – are the same factors thought to be needed to improve the performance of ceria-based desulfurization sorbents. Therefore, the objective of the current research is to determine if ceria-zirconia sorbents are capable of achieving Vision 21 desulfurization goals in typical coal gas compositions.

1.3. Objectives of the Research

The project is divided into two major activities – the electrochemical synthesis and characterization of CeO₂-ZrO₂ mixtures and high temperature desulfurization using CeO₂-ZrO₂ sorbents. Electrochemical synthesis and characterization, and construction of a laboratory-scale fixed-bed reactor suitable for determining sub-ppmv H₂S

concentrations were emphasized during year 01. These topics were described in detail in the first annual report (Mukherjee et al. 2001); only brief summaries are repeated in this report. While the electrochemical synthesis work was successful, it proved to be impossible to produce sufficient quantities of material to properly evaluate the desulfurization potential. Characterization and testing of commercially available CeO_2 and $\text{CeO}_2\text{-ZrO}_2$ materials were emphasized in the annual report from year 02 (Yi et al. 2002); this work is also summarized in this report. Primary attention during year 03 turned to the preparation of CeO_2 and $\text{CeO}_2\text{-ZrO}_2$ sorbents in this laboratory, the characterization of these sorbents, and desulfurization tests using these in-house sorbents. This work is emphasized in this annual report.

2. ELECTROCHEMICAL SYNTHESIS AND CHARACTERIZATION OF $\text{CeO}_2\text{-ZrO}_2$

Switzer (1987) and Yanchun et al. (1995) have recently demonstrated the electrochemical synthesis of CeO_2 and ZrO_2 , respectively, but there has been no previous work on the electrochemical preparation of $\text{CeO}_2\text{-ZrO}_2$ mixtures. In this study, the powders were co-deposited and the chemical composition, phase structure, and crystallite size of the mixture was studied as a function of the processing parameters. Conditions were identified for producing ceria-zirconia mixtures that exhibit solid solutions of the fluorite-type structure, are nanocrystalline, and contain about 25mol % zirconia.

2.1. Electrochemical Experimental

Figure 1 shows the two-compartment electrochemical cell employed in the powder synthesis. The anolyte and catholyte were separated by a glass frit. A platinum mesh was used as the anode. The reference electrode was a saturated calomel electrode (SCE). An inverted, stationary, stainless steel shaft-disk electrode was used as described by Podlaha et al. (1997) with the electrode surface facing upwards in the electrolyte to avoid blockage of the electrode surface by trapped H_2 gas bubbles produced from water and proton reduction. The stainless steel disc electrodes (AISI 304L) were embedded inside an epoxy resin such that only one side was exposed to the electrolyte. A thin, stainless steel shaft, encased in Teflon, was screwed into the disc-epoxy assembly. The shaft was threaded allowing electrical contact to the disc.

The electrolyte consisted of 0.5 M ammonium nitrate, and varying concentrations of zirconyl (IV) nitrate hydrate and cerium (III) nitrate hexahydrate. All experiments were carried at room temperature of 23 ± 1 °C. Table 1 lists the different compositions of the electrolyte used. The pH was maintained at 1.5 ± 0.1 at the start of each experiment. The deposited powders were scraped from the electrode, dried in a desiccator at room temperature, and analyzed.

2.2. Solid State Analyses

The chemical composition of the deposits was measured by energy dispersive x-ray fluorescence spectroscopy (EDXRF) calibrated with bulk samples of ceria and zirconia.

The composition was determined over a large region of pressed sorbent powder to verify uniformity of the ceria-zirconia mixture. Four to five measurements were averaged for each sample. Once the powder concentration was found in the desired range of 15-50 mol % zirconia, further analysis by x-ray diffraction (XRD) and transmission electron microscopy (TEM) was carried out to verify the structure of the material. The crystallinity and particle size of the as-produced powder were analyzed by a bright-field high resolution TEM. The phase identification of the sample and the lattice parameters were determined with x-ray diffraction analysis (XRD). Intensity data were collected at ambient temperature in the 2θ range between 25° and 60° , and the peaks of each compound were compared with phases in the International Center for Diffraction Data database (ICDD).

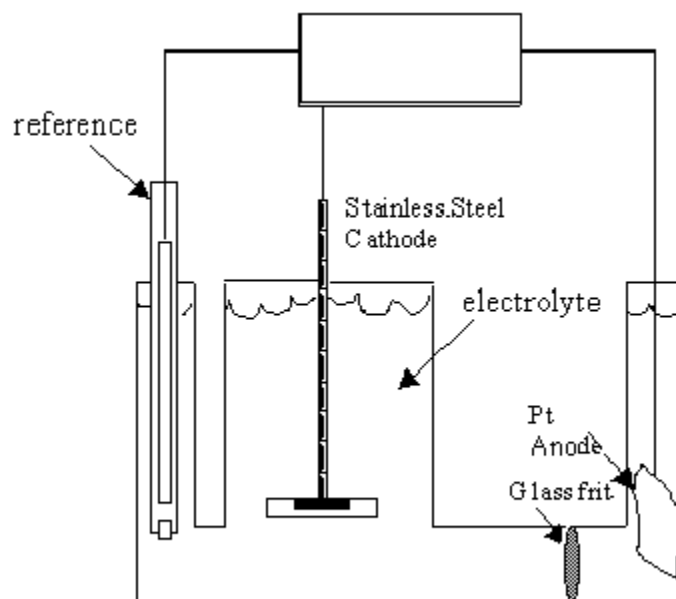


Figure 1. Electrochemical Cell Schematic

Table 1. Composition of the Various Electrolyte Solutions.

Electrolyte	$\text{Ce}(\text{NO}_3)_3 \cdot 6\text{H}_2\text{O}$	$\text{Zr}(\text{NO}_3)_4 \cdot \text{H}_2\text{O}$	NH_4NO_3 (M)
A	0.5	0.0	0.5
B	0.5	0.1	0.5
C	0.5	0.2	0.5
D	0.25	0.2	0.5
E	0.125	0.2	0.5
F	0.25	0.5	0.5
G	0.125	0.5	0.5

2.2.1. Composition

Figure 2 shows that the final powder composition is a linear function of the initial electrolyte concentration at various applied potentials. At low Zr concentrations in the electrolyte ceria is preferentially deposited over zirconia, which diminishes as the Zr

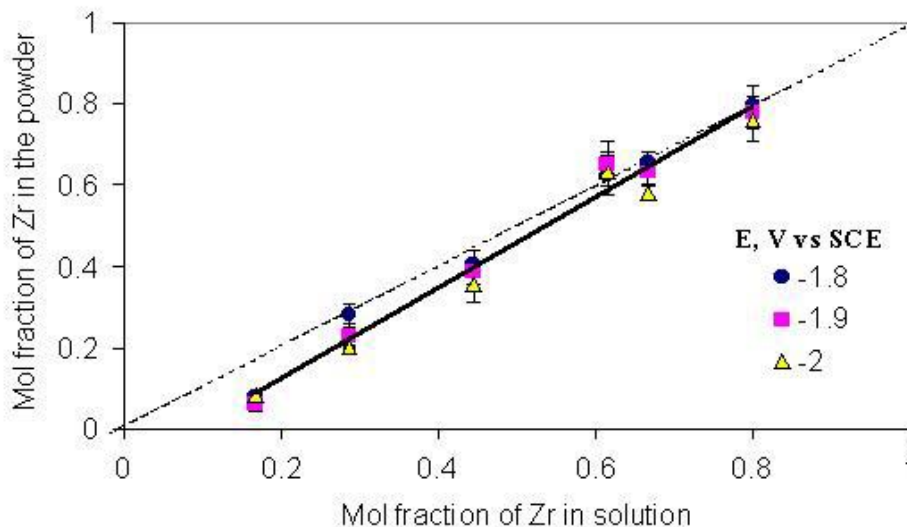


Figure 2. Electrolyte Concentration vs. Final Powder Composition

concentration of the solution increases. The powder composition was independent of the applied potential. As a reference point, a dashed line has been added to Figure 2 to show the 1:1 correspondence between the mol fraction of Zr in the powder with concentration in solution.

2.2.2. XRD and TEM Characterization

Figure 3 shows high-resolution TEM images of the CeO_2 and $\text{CeO}_2\text{-ZrO}_2$ samples. The average grain diameters of the nanocrystallites were approximately 5 nm, independent of composition. Crystallite size of this order compares favorably with many of the standard wet and dry processing production methods. Selected-area electron diffraction (SAED) patterns indicated a crystalline material and suggested the presence of a solid solution.

The crystallite size and phase were also verified with X-ray diffraction (XRD). The XRD of the powder sample having 18 at % Zr is shown in Figure 4(a) and compared to the standard library patterns of cubic CeO_2 (b) and monoclinic and tetragonal ZrO_2 (c). The spectrum exhibits a cubic single phase similar to solid solution $\text{ZrO}_2\text{-CeO}_2$ XRD patterns of samples generated by non-electrochemical techniques. The mean crystal size, calculated from the full width at half maximum of the (111) reflection, was 4.5 nm, which is consistent with the TEM observation. As the concentration of ZrO_2 increased a

second phase corresponding to ZrO_2 began to emerge. Formation of a separate ZrO_2 phase is thought to be undesirable for a desulfurization sorbent.

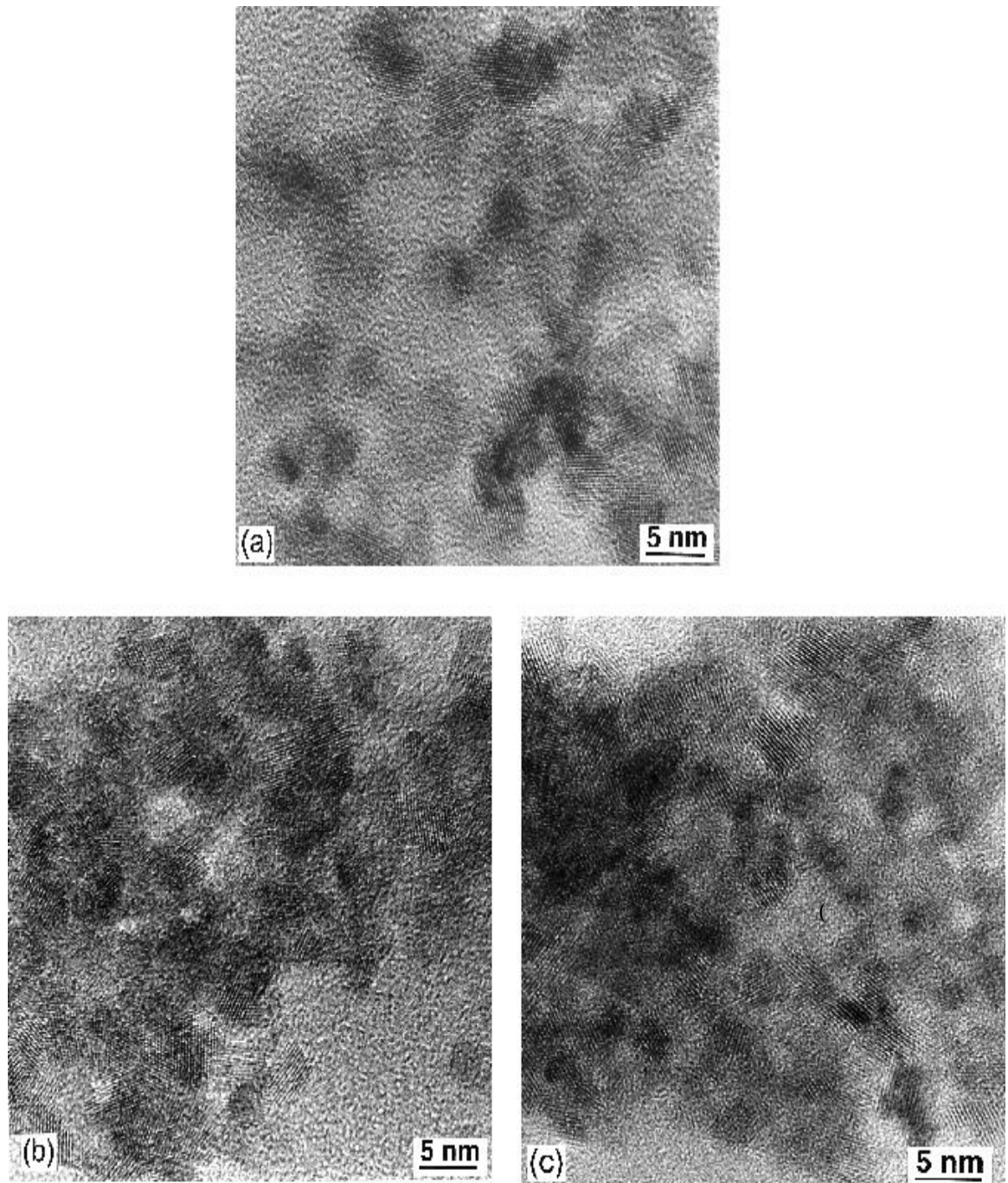


Figure 3. TEM images of (a) Ceria, (b) Ceria-7 at.% Zirconia (C) Ceria-18 at.% Zirconia

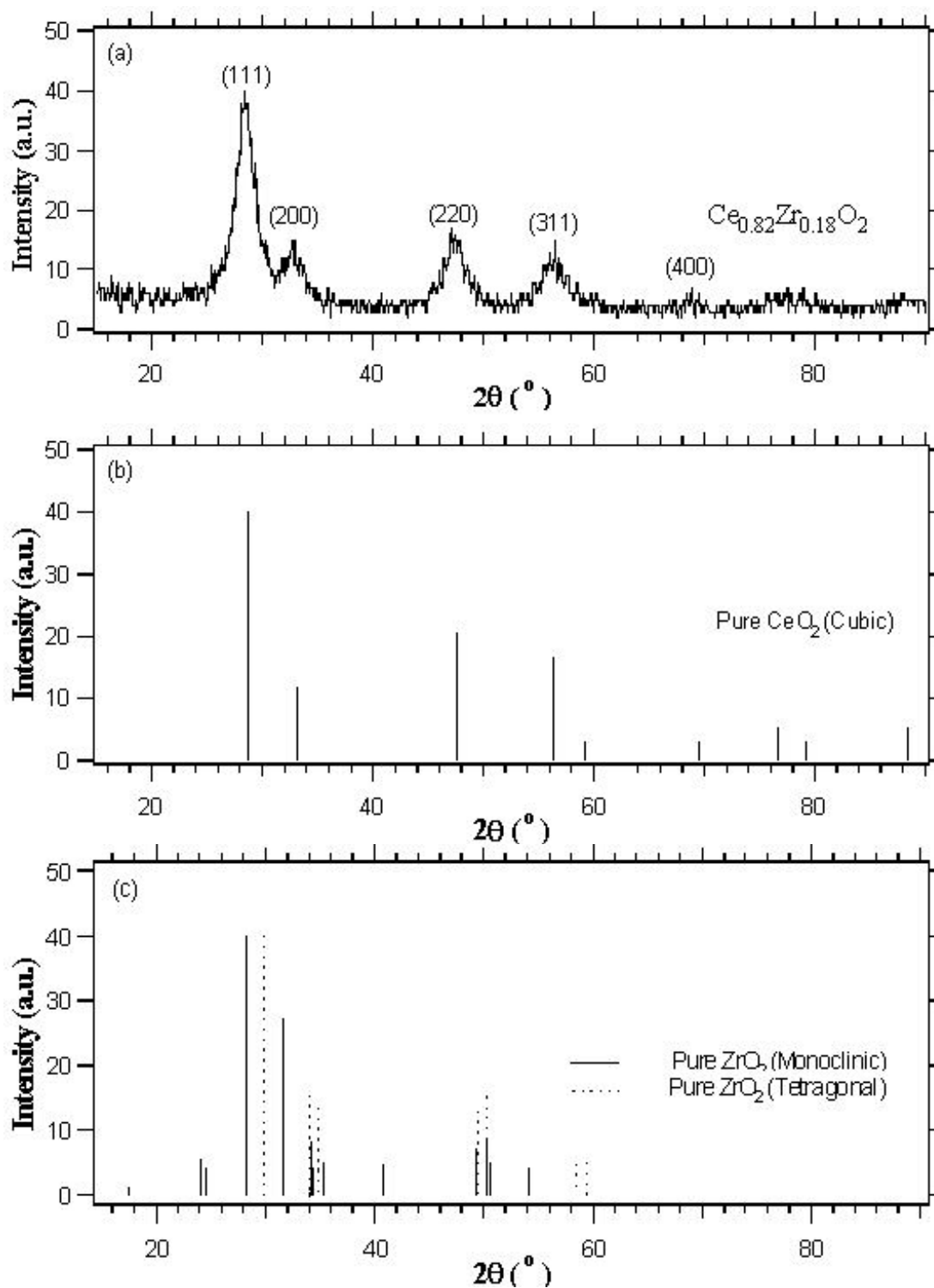


Figure 4. XRD Analysis of (a) Electrochemically Generated Nanocrystalline $\text{Ce}_{0.82}\text{Zr}_{0.18}\text{O}_2$, (b) Cubic CeO_2 (JCPDS 34-394), and (c) Monoclinic (JCPDS 37-1484) and Tetragonal (JCPDS 42-1164) ZrO_2

The solid solution must be stable at high temperature if the material is to serve as a good sorbent. The XRD patterns of a sample containing 18.7 mol % ZrO_2 heat treated at 700°C for varying times are shown in Figure 5. Heat treatment was carried out for a specified time on a single sample, which was then cooled to room temperature and subjected to XRD analysis. The procedure was repeated with the following heating times: 2, 2, 3, 5, 10, 24, 60 hr (cumulative time of 106 hr). The Al peak in Figure 5 came from the sample holder and was not part of the powder. No phase separation was observed.

The particle size increased slightly with prolonged heat treatment steps, and after 106 hours of heating at 700°C , the crystallite size was 14.5 nm. Large increases in crystallite size are not considered desirable, but the increase observed was small enough that it is not considered critical for sorbent performance. A TEM micrograph following heat treatment for 106 hours, verified the increase in crystallite size observed with XRD.

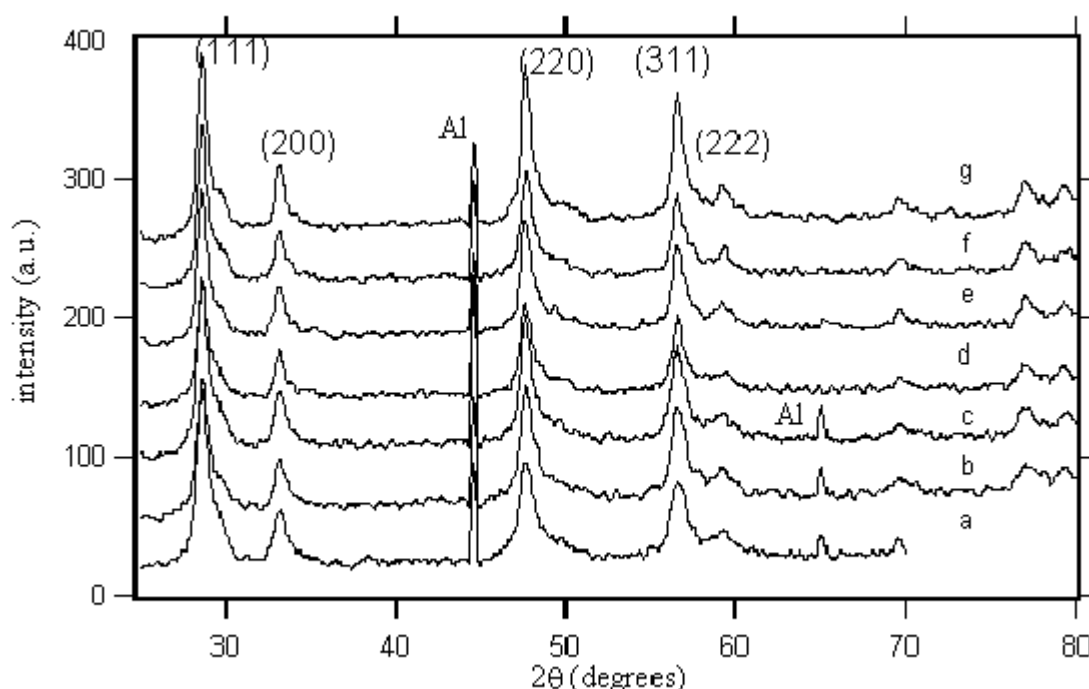


Figure 5. Heat Treated 700°C , 18.7 mol % Zr Ceria-Zirconia with Resulting Crystallite Size of (a) 9.5 nm, (b) 10 nm, (c) 11 nm, (d) 12 nm, (e) 12.5 nm, (f) 12.5 nm, and (g) 14.5 nm.

3. HIGH TEMPERATURE DESULFURIZATION TEST EQUIPMENT

3.1. Fixed-Bed Reactor

Sorbent performance during H_2S removal is evaluated using the fixed-bed reactor system shown in Figure 6. Gases – H_2S , H_2 , N_2 , and CO_2 – are obtained from high purity cylinders and flow rates are controlled using calibrated mass flow controllers. The proportions of H_2 and CO_2 in the feed gas can be adjusted to control the reducing power (oxygen partial pressure) of the feed gas. Valves are arranged so that either feed or

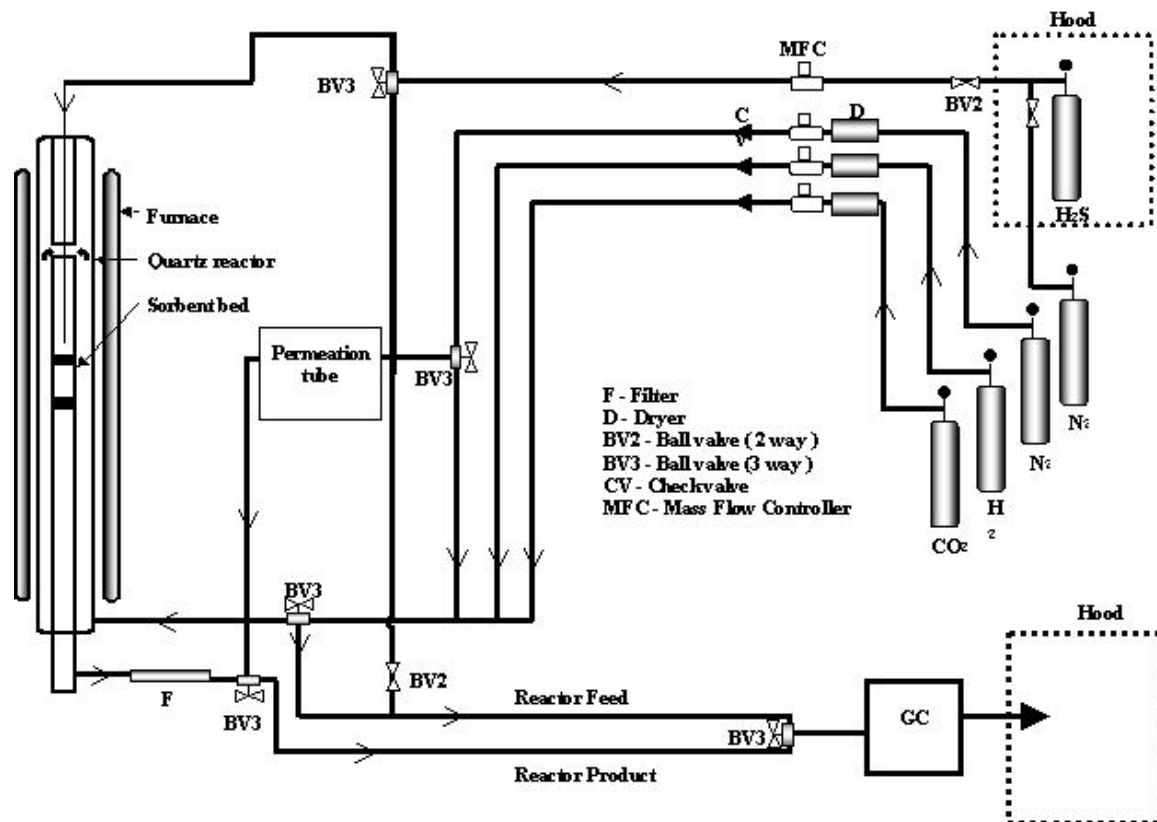


Figure 6. Fixed-Bed Reactor System

product gas can be fed to the gas chromatograph for analysis. In addition, N₂ feed gas can be directed past a calibrated H₂S permeation tube where a standard quantity of H₂S is added for calibration of the gas chromatograph at low H₂S concentrations (< 10 ppmv). Calibration at higher H₂S concentrations is accomplished by mixing pure cylinder gases using the mass flow controllers.

In normal operation H₂, CO₂, and N₂ are mixed in the desired proportions and fed to the bottom of the quartz reaction vessel. These gases are preheated as they flow upward in the annular region outside of the reactor insert. H₂S is added to the preheated gases just before they contact the sorbent bed, which is supported inside the reactor on a porous quartz disc and quartz wool. Sorbent pre-reduction, if used, is carried out in the same manner except that H₂S is not added. Product gas exits from the bottom of the reactor, and flows through a quartz wool filter to remove any particulate matter and/or traces of elemental sulfur that may be present, and to the gas chromatograph for analysis.

All components of the reactor vessel and insert and all valves are of quartz or Teflon to prevent interaction between low concentrations of H₂S and steel surfaces. Steel surfaces within the gas chromatograph are silcosteel to eliminate interaction. The only untreated steel surfaces that contact H₂S are the feed gas lines.

A more detailed diagram of the quartz reactor, including dimensions, is shown in Figure 7. The total capacity of the reactor is approximately 15 g of solid.

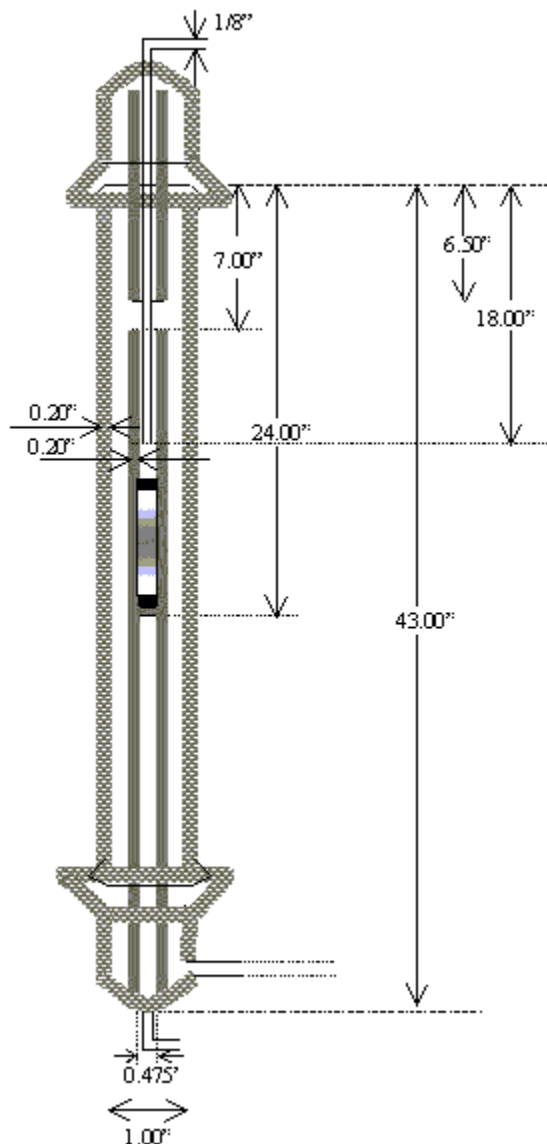


Figure 7. Details of the Quartz Reactor

3.2. Gas Analysis

H₂S concentration of the feed and product gas is determined using a Varian model 3800 gas chromatograph purchased for this project using LSU matching funds. The chromatograph is equipped with dual columns, two Valco multiport sampling valves, and both a pulsed flame photometric detector (PFPD) and a thermal conductivity detector (TCD). The PFPD is used for H₂S concentrations from sub-ppmv to about 10 ppmv, while the TCD is used for concentrations in excess of 100 ppmv. There is a gap in the analytical capability between about 10 and 100 ppmv, but primary interest is in the low concentration range. The PFPD provides analytical capability to approximately 0.1 ppmv

Table 2. Gas Chromatograph Operating Conditions

PFPD	Column:	CP SIL5, 5 μ
		L = 3 m, D = 530 μ , T = 200°C
	Carrier Gas:	He, 2.9 ml/min
	Sample Loop:	SilcoSteel, 50 μ L
TCD	Column:	HAYESEP A SilcoSteel
		L = 3.3 m, D = 3.13 μ , T = 200°C
	Carrier Gas:	He, 28 ml/min
		He, 31.2 ml/min (backflush)
	Sample Loop:	SilcoSteel, 2 ml

H₂S (100 ppbv) and is about 10 times more sensitive than a standard flame photometric detector. A summary of chromatograph operating conditions is presented in Table 2.

The flow arrangement through the two automatic valves (one 10-port and one 6-port) is shown in Figure 8. The upper left diagram shows gas flows in normal operation. The gas to be analyzed enters the 10-port valve at position 4, exits to the PFPD sample loop at position 5, re-enters the 10-port valve at position 8, exits to the TCD sample loop at position 9, again enters the 10-port valve at position 2 and is vented to a laboratory hood through position 3. In this operation mode the contents of both sample loops are continually purged and replenished with the most recent product gas. Three carrier gases are used. Carrier 1 enters the 10-port valve at position 7 and exits at position 6 to the PFPD column and then to the PFPD. Carrier 2 enters the 10-port valve at position 10, exits at position 1, and flows to the 6-port valve. It enters the 6-port valve at position 2 and exits through position 1 to the TCD column, then back into the 6-port valve at position 3 and out through position 4 to the TCD and laboratory vent. Carrier 3 enters the 6-port valve at position 5 and exits through position 6 to vent.

Samples for both the PFPD and TCD are acquired simultaneously by switching the 10-port valve to the position shown in the upper right diagram of Figure 8. The product gas sample enters the 10-port valve at position 4 and exits through position 3 directly to the laboratory vent. Carrier gas 1 enters the 10-port valve at position 7, exits through position 8 and picks up the sample from the PFPD sample loop. It reenters the 10-port valve at position 5 and exits through position 6 to the PFPD column. Column effluent then flows directly to the PFPD. Carrier gas 2 enters at position 10 and exits through position 9 where it picks up the TCD sample. It re-enters the 10-port valve at position 2 and exits through position 1 to the 6-port valve. The TCD sample enters the 6-port valve at position 2 and exits to the TCD column through position 1. The TCD column effluent re-enters the 6-port valve at position 3 and exits through position 4 to the TCD. Flow of carrier 3 is unchanged. It enters the 6-port valve at position 5 and exits through position 6 to vent.

The position of the 6-port valve is switched in the lower center diagram of Figure 8 to permit H₂O formed during the desulfurization reaction to be backflushed to vent. Switching occurs after H₂S has been eluted from the TCD column but before water is

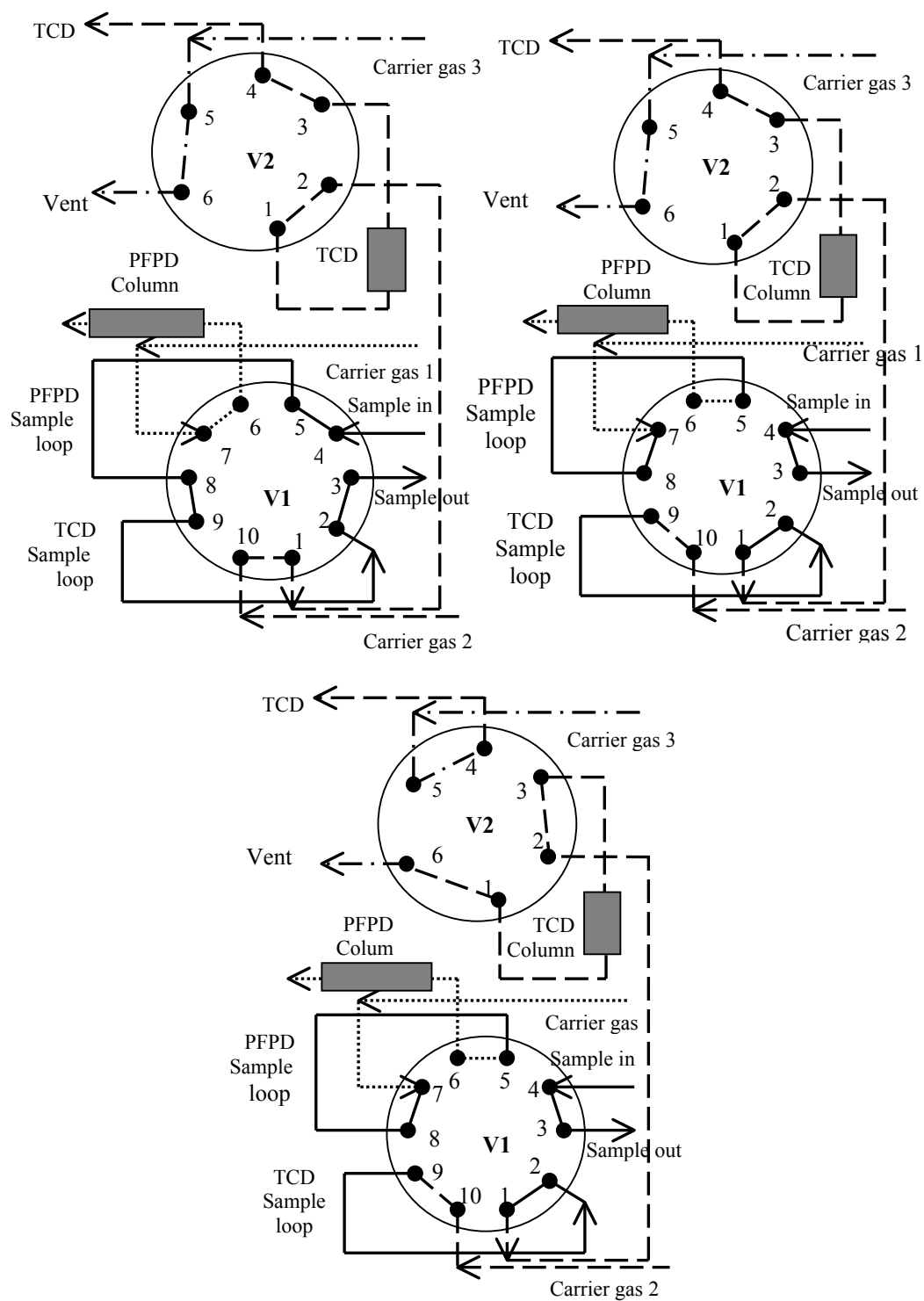


Figure 8. Chromatograph Sampling Arrangement

eluted. Sample gas and carrier gas 1 flows are not changed from the previous case. However, with the 6-port valve in the new position, carrier gas 2 flows through the 10-port valve as before. It enters the 6-port valve at position 2, exits through position 3, and flows in the reverse direction through the TCD column to backflush the H₂O. Carrier gas 2 plus the H₂O then re-enters the 6-port valve at position 1 and exits through position 6 directly to vent. Carrier gas 3 enters the 6-port valve at position 5 and exits through position 4 to the TCD so that carrier gas flow is maintained through the TCD at all time.

PFPD calibration was accomplished by flowing N₂ at a known rate past a calibrated H₂S permeation tube maintained at 30°C (see Figure 6). A PFPD calibration curve between 0.1 and 6 ppmv H₂S is shown in Figure 9. The chromatogram obtained from the 0.1 ppmv H₂S sample shown in Figure 10 indicates that the signal-to-noise ratio is strong even at this low H₂S concentration. The best calibration was obtained by correlating H₂S peak height versus H₂S concentration using a third order polynomial with a zero intercept. The calibration equation shown on the figure has a R² value of 0.9982.

TCD calibration was accomplished by mixing N₂ and H₂S from the high purity cylinders with flow rates controlled using the mass flow controllers. Results of the TCD calibration between 100 ppmv and 1.5% (15,000 ppmv) are shown in Figure 11. The calibration was also based on H₂S peak height using a second order polynomial with a zero intercept and the R² value was 0.9996.

Calibration curves are checked periodically and the detectors are recalibrated when necessary.

4. SORBENT MATERIALS

Because it was impossible to produce sufficient quantities of CeO₂ and CeO₂-ZrO₂ needed for desulfurization testing using electrochemical synthesis, a number of sorbent materials from other sources have been acquired and screened for desulfurization performance. Test materials have been acquired from Rhone Poulenc, NexTech Materials, Alfa Aesar and have been synthesized in the LSU laboratory using a co-precipitation technique. The initial screening tests used commercial materials obtained from outside sources. These materials were prepared using different techniques and had different properties. Results indicated that sorbents having similar properties would be required if the effects of ZrO₂ addition were to be evaluated. Because of the need for the sorbents having similar properties, later work concentrated on materials synthesized at LSU. All materials were characterized in terms of their x-ray diffraction patterns, specific surface area, and reducibility in addition to their ability as a H₂S sorbent.

4.1 Commercial Sorbents

A total of six CeO₂ and CeO₂-ZrO₂ compounds obtained from Rhone Poulenc, Alfa Aesar, and NexTech Materials have been acquired and subjected to selected characterization and desulfurization tests. A list of these compounds with selected properties is presented in Table 3. Surface areas of the as-received materials were either

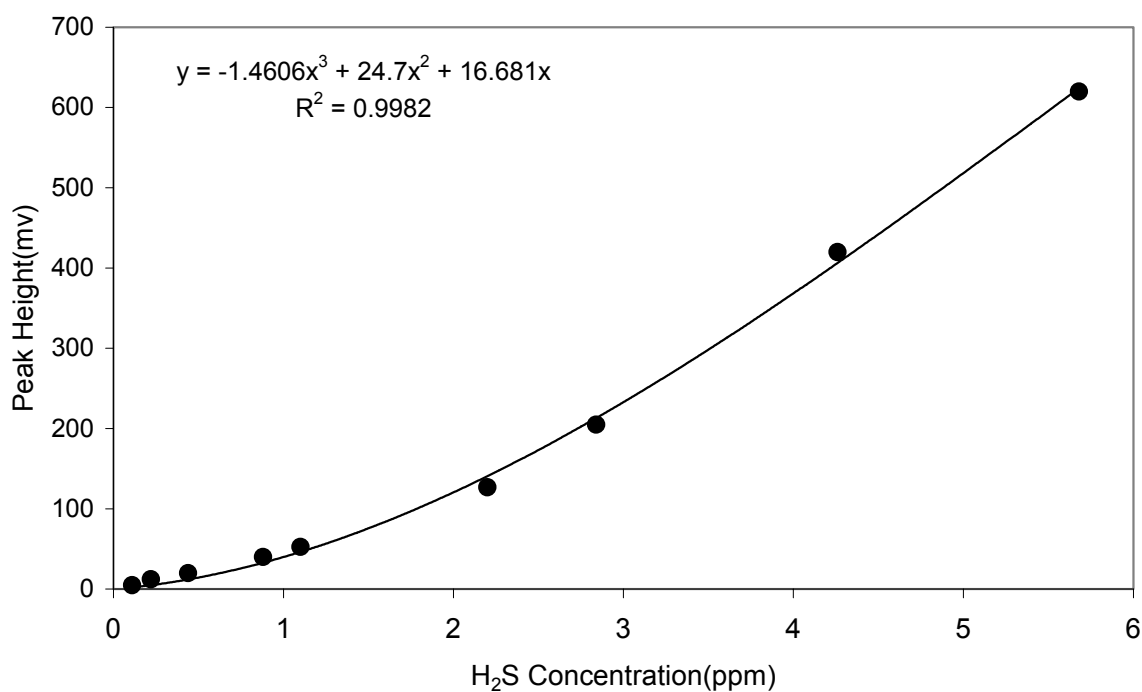


Figure 9. PFPD Calibration Curve

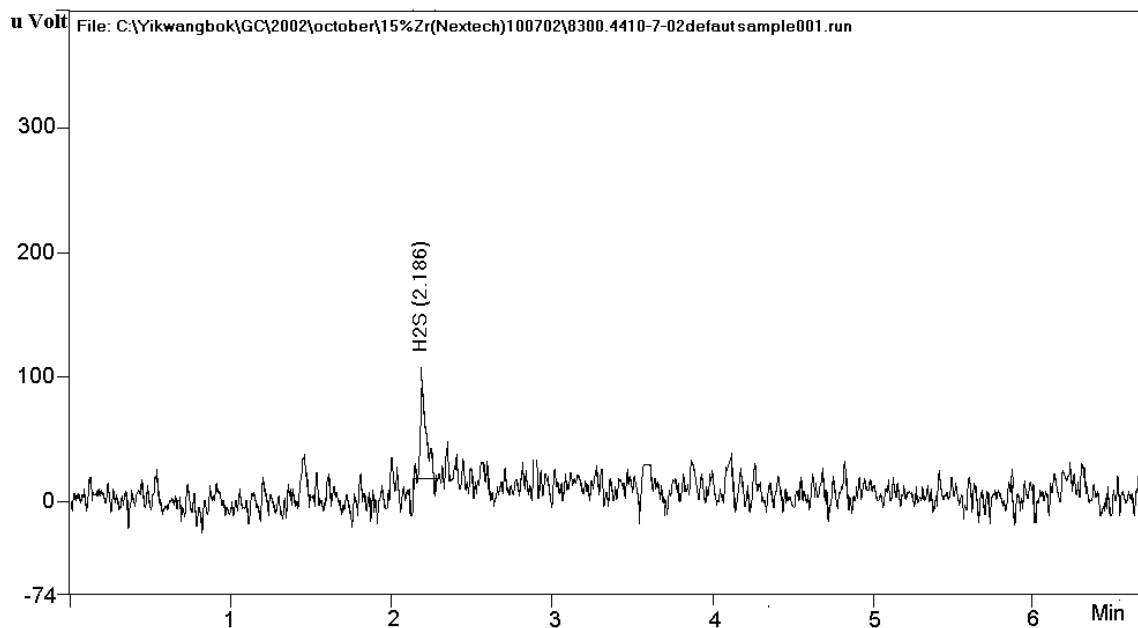


Figure 10. PFPD Chromatogram at 0.1 ppmv H₂S

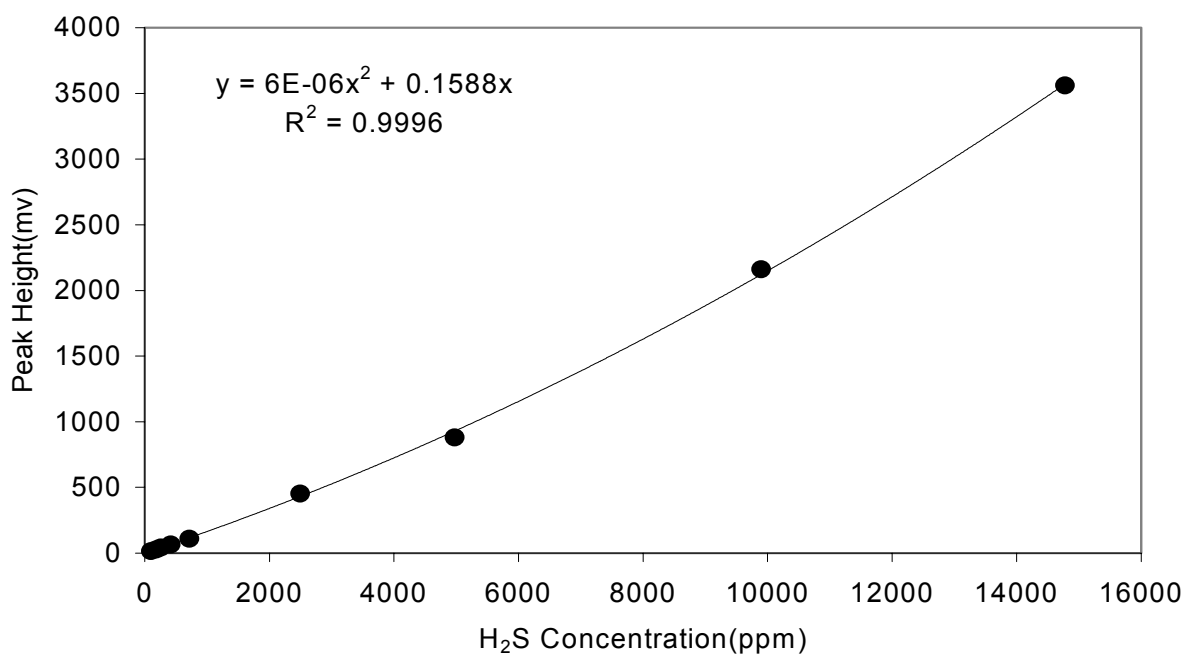


Figure 11. TCD Calibration

Table 3. Commercial CeO₂ and CeO₂-ZrO₂ Materials and Selected Properties

Compound/Source/Designation	Surface Area, m ² /g		Crystallite Size, nm
	As-Received	Calcined*	
CeO ₂ /Rhone Poulenc/Ce(RP)	210	110	3
CeO ₂ /Alfa Aesar/Ce(Alfa)	40	45	25
Ce ₂ (CO ₃) ₃ ·xH ₂ O/Alfa Aesar/CeC(Alfa)	50	40	NA
85%CeO ₂ -15%ZrO ₂ /NexTech/CZ(Nex)85	105	80	9
80%CeO ₂ -20%ZrO ₂ /NexTech/CZ(Nex)80	145	NA	9
70%CeO ₂ -30%ZrO ₂ /NexTech/CZ(Nex)70	124	70	NA

* at 700°C for 4 hr in N₂

NA not available

measured at LSU or reported by the manufacturer, while all surface areas following calcination were determined at LSU. Crystallite sizes were determined at LSU based on line broadening analysis of the 111 XRD peak. In the following sections of this report these sorbents are referred to by the designations found in Table 3, i. e., CeO₂ from Rhone Poulenc is referred to as Ce(RP).

The CeO₂ from Rhone Poulenc (Ce(RP)) is the same material used in the earlier studies at LSU (Zeng et al. 1999 and Zeng et al. 2000). The as-received material is considered to be 91% CeO₂ since it experiences a 9% weight loss when heated to high temperature in an inert gas. The surface area of the as-received material is based on data

from Zeng while crystallite size and surface area following calcination were measured in this project.

Properties of the CeO_2 and $\text{Ce}_2(\text{CO}_3) \cdot x\text{H}_2\text{O}$ from Alfa Aesar (Ce(Alfa) and CeC(Alfa)) were determined at LSU. The purity of the Ce(Alfa) was 99.5%. Upon calcination, the CeC(Alfa) should decompose to CeO_2 . We were interested in this compound as a possible sorbent precursor because of the possibility that the calcined material would have an extremely large surface area and therefore be extremely reactive. As shown in Table 3, the high surface area did not develop.

Approximately 50g each of three CZ(Nex) samples were donated by NexTech Materials for the project. These amounts were sufficient for characterization and desulfurization screening, but not for complete desulfurization testing where between 2 and 6 g of sorbent was required for each test. The x-ray diffraction spectrum of CZ(Nex)80 presented in Figure 12 shows no significant difference from the spectrum of the 78% CeO_2 -18% ZrO_2 material prepared electrochemically at LSU and shown in Figure 5. The most important result is that there is no indication of a separate ZrO_2 phase in either of the spectra.

Only the Alfa Aesar products were available in the quantities needed for desulfurization testing and, as shown in Table 4, their surface areas were considerably smaller and crystallite sizes considerably larger than the other materials. In addition, only one CeO_2 - ZrO_2 composition was available from Alfa Aesar. Because of these limitations we began to prepare CeO_2 and CeO_2 - ZrO_2 compounds at LSU. These materials are described in the following section.

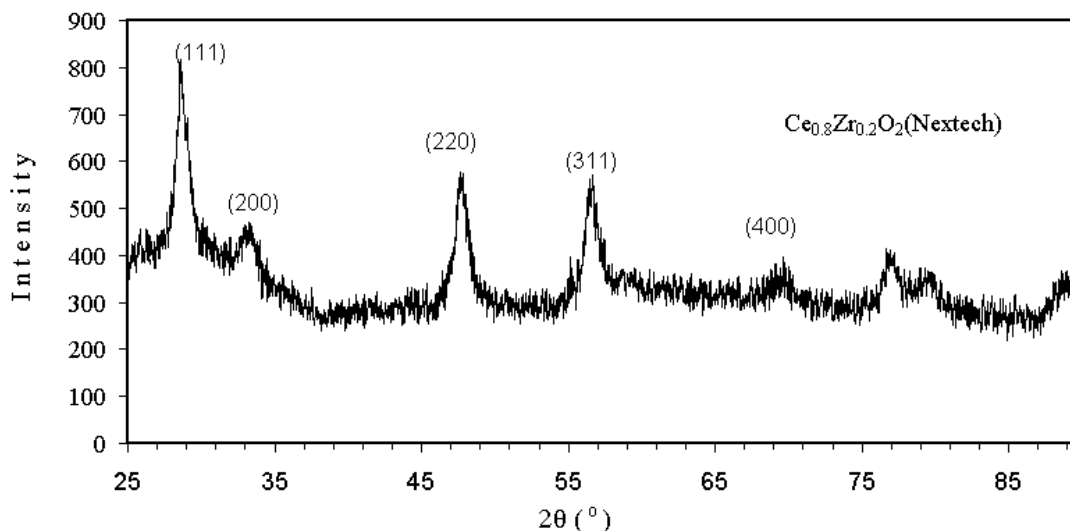


Figure 12. XRD Spectrum of CZ(Nex)80

4.2. LSU Sorbents

CeO_2 and two CeO_2 - ZrO_2 compounds were synthesized using the co-precipitation technique described by Rossignol et al. (1999). An aqueous solution containing desired

proportions of cerium (III) nitrate hexahydrate and zirconyl nitrate hydrate was prepared. The mixture was held at 50°C for 30 minutes to insure complete solution. Precipitation was induced by slowly adding an excess of 25% NH₄OH solution. The temperature was then raised to 100°C where the liquid slowly evaporated over a period of about 4 to 5 hours. The dried powder was calcined at 400°C for 2 hours. The calcined product was then crushed and sieved with the 150 – 300 µm fraction retained for testing.

Properties of these materials, which are summarized in Table 4, lie between those of the Alfa Aesar and NexTech materials. Since the properties are also reasonably independent of composition, the majority of the desulfurization tests during year 03 used these LSU-prepared sorbents. The sorbent designations in Table 4 are used in the following sections to identify these materials.

XRD spectra for the Ce(LSU) and CZ(LSU)80 are compared in Figure 13. The two spectra are essentially identical and there is no indication of a separate ZrO₂ phase. In addition, these spectra are also effectively identical to those in Figures 5 and 11.

Table 4. CeO₂ and CeO₂-ZrO₂ Materials Prepared at LSU by Coprecipitation

Compound/Designation	Surface Area, m ² /g		Crystallite Size, nm
	As-Prepared	Calcined*	
CeO ₂ /Ce(LSU)	75	35	16
90%CeO ₂ -10%ZrO ₂ /CZ(LSU)90	75	50	13
80%CeO ₂ -20%ZrO ₂ /CZ(LSU)80	85	55	19

* at 400°C for 2 hrs in N₂

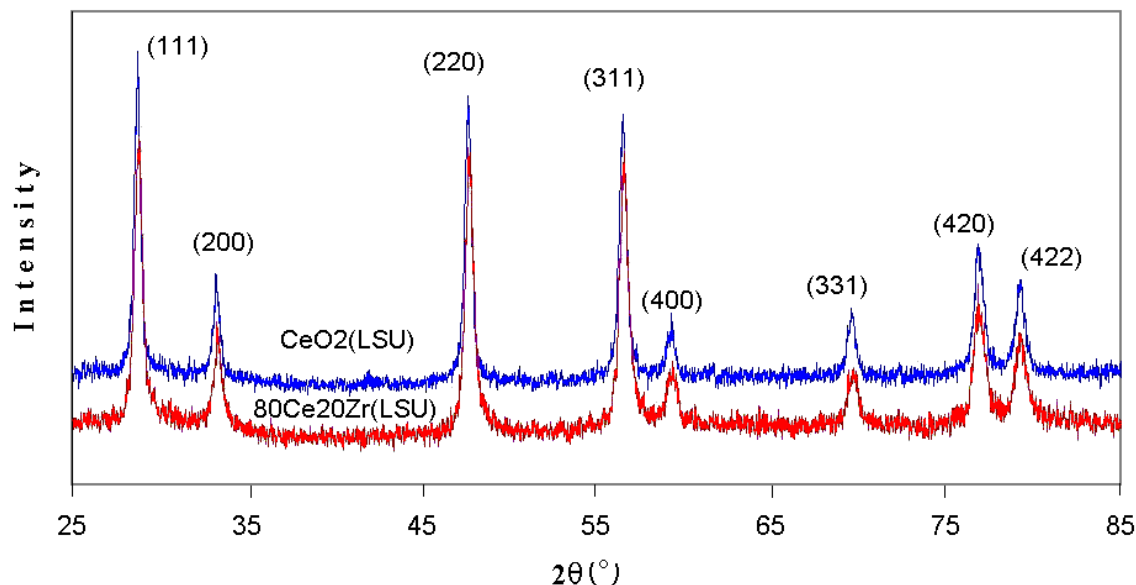


Figure 13. XRD Spectra of CZ(LSU)80 and Ce(LSU)

5. SORBENT REDUCTION

The ability to reduce CeO_2 to CeO_n ($1.5 < n < 2.0$) has been studied using an electrobalance reactor. In these tests the sorbent was initially exposed to an inert atmosphere and heated to 800°C until the weight became constant. Weight loss in the inert atmosphere due to loss of volatile material from the solid was considered in the sulfidation analysis. The sample was then cooled and subsequently heated slowly in a reducing atmosphere to 1000°C . Weight loss in the reducing atmosphere is directly related to the value of n in CeO_n . Sorbents were tested using three different reducing gas compositions:

Gas 1	10% H_2 , 0.0% CO_2 , balance He
Gas 2	10% H_2 , 3.5% CO_2 , balance He
Gas 3	50% H_2 , 3.5% CO_2 , balance He.

The equilibrium partial pressure of O_2 provides a measure of the reducing power of the gas. Gas 1 is oxygen free except for trace impurities present in the H_2 and He, and has, in principle, the greatest reducing power. The presence of CO_2 in the other gases provides small quantities of free O_2 at elevated temperatures and the ratio of H_2 to CO_2 determines the amount of free O_2 and the reducing power. Results of equilibrium partial pressure calculations for Gases 2 and 3 as a function of temperature, performed using HSC Chemistry, are shown in Figure 14. The equilibrium O_2 pressure ranges from about 10^{-32} atm at 400°C to 10^{-14} atm at 1000°C , with the equilibrium O_2 pressure being 1 to 2 orders of magnitude lower in reducing Gas 3. At 700°C , the most common experimental desulfurization temperature in the experiments tests, the equilibrium O_2 pressures are about 10^{-21} and 10^{-20} atm for Gases 3 and 2, respectively

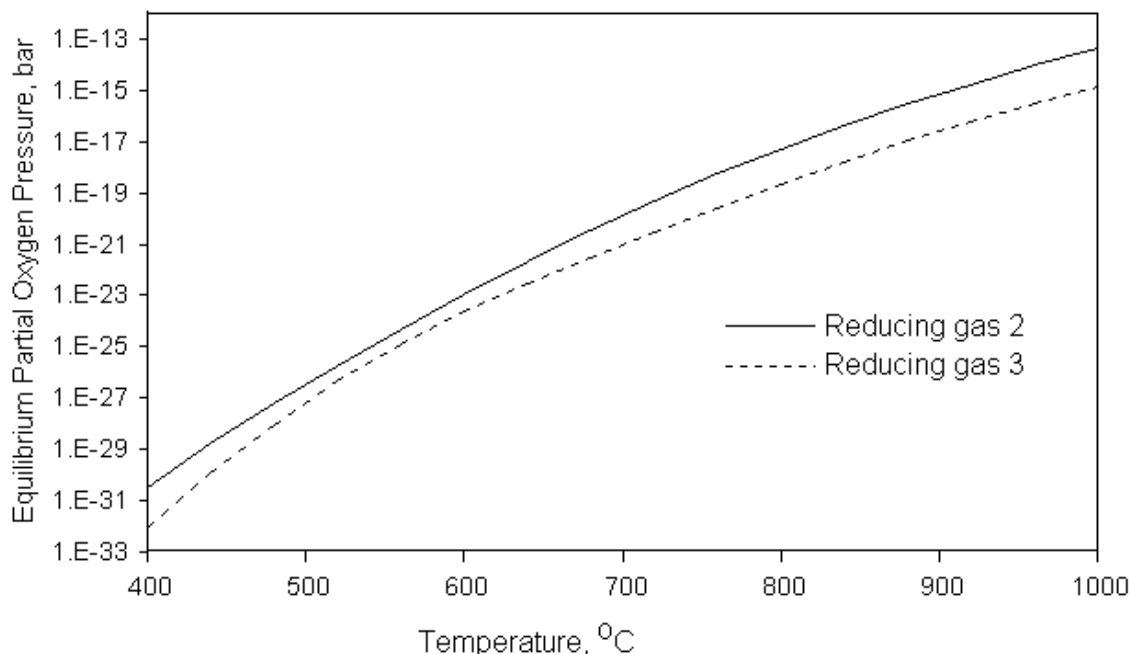


Figure 14. Equilibrium Oxygen Pressure in Reducing Gases 2 and 3.

5.1. Commercial Sorbents

Reduction results in the three reducing gases using Ce(RP) are compared in Figure 15 where the value of n in CeO_n is plotted as a function of temperature. In Gas 1 (most highly reducing) reduction began at about 650°C and the value of n at the final 1000°C temperature was 1.81. In Gas 3 having intermediate reducing power reduction began near 700°C and the final value of n was 1.85. In the least reducing Gas 2 reduction also began at about 700°C and the final value of n was 1.88. The difference in the level of reduction in Gases 2 and 3 became appreciable at about 750°C. These values of n are in reasonable agreement with experimental values published by Bevan and Kordis (1964) based on the O_2 pressures of Figure 14.

The reducibility of Ce(RP) and CZ(Nex)80 are compared in Figure 16 using the most highly reducing Gas 1. Reduction of CZ(Nex)80 began near 300°C compared to about 650°C for Ce(RP). The final values of n at 1000°C were 1.75 for CZ(Nex)80 and 1.81 for Ce(RP). These tests provided the first experimental proof that ZrO_2 addition increases the reducibility of CeO_2 .

The results shown in Figures 15 and 16 are typical of all reduction results using the commercial sorbents as shown by the data summary presented in Table 5. The temperatures corresponding to values of $n = 1.98$, 1.86, and 1.80 as well as the values of n at the most common sulfidation temperature of 700°C and the final reduction temperature of 1000°C are presented for six test materials using the three reducing gases. Roughly speaking, the temperature corresponding to $n = 1.98$ represents the beginning of reduction for each sorbent, while the temperature for $n = 1.86$ is at an intermediate

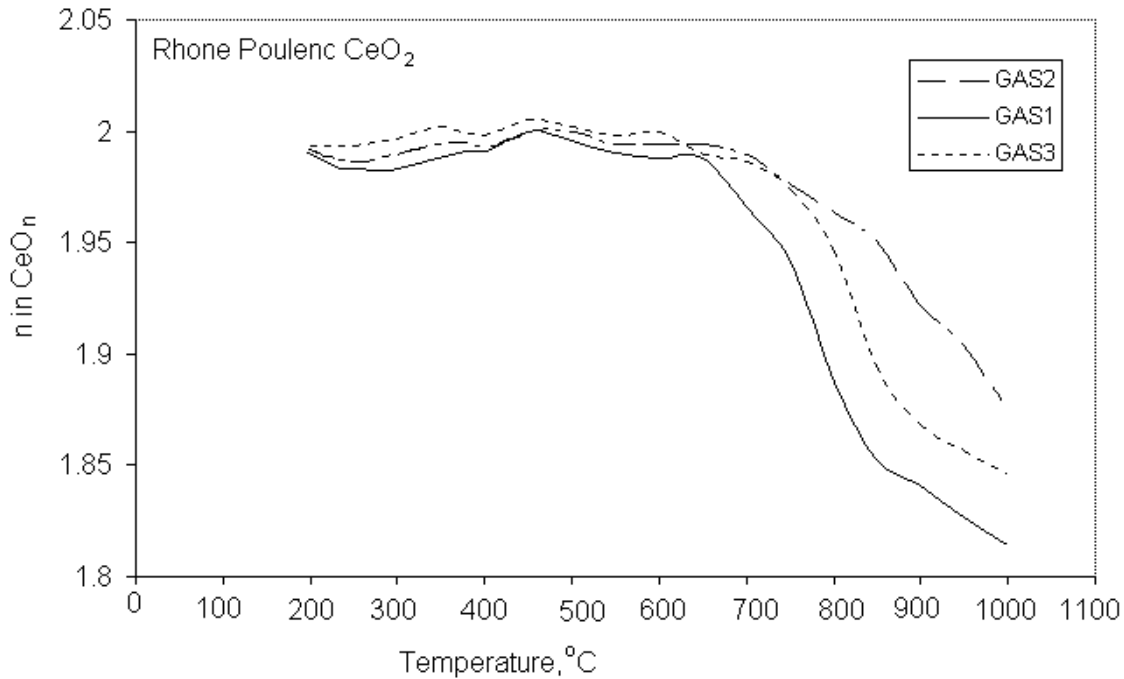


Figure 15. Reduction of Ce(RP)

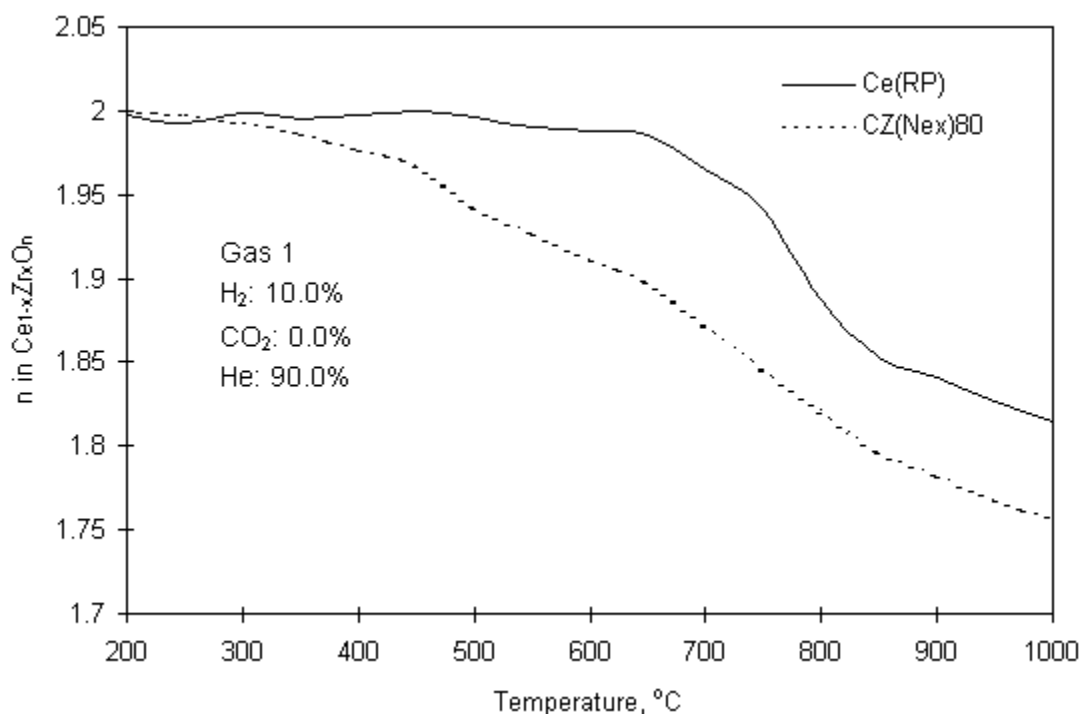


Figure 16. Comparison of Reducibility of Ce(RP) and CZ(Nex)80 in Reducing Gas 1.

condition of reduction for CeO₂-ZrO₂ sorbents and near the end of reduction of CeO₂ materials. Finally, the temperature for $n = 1.76$ is near the end of reduction for most of the CeO₂-ZrO₂ sorbents. Table 5 clearly shows that the materials from Alfa are the most difficult to reduce while the CeO₂-ZrO₂ materials from NexTech are the most easily reduced. Reduction of the NexTech materials begins at about 300°C and final values of $n \approx 1.75$ were achieved for all three NexTech sorbents in the most strongly reducing gas, and in all three gases for the material containing 30% ZrO₂.

5.2. LSU Sorbents

Reduction results for the three LSU sorbents in Gas 3 (intermediate reducing power) are presented in Figure 17 and a summary of all reduction test results is found in Table 6. In Figure 17 we see that, while there is very little difference in the reducibility of the two sorbents containing ZrO₂, both are subject to considerably higher levels of reduction than CeO₂ with no added ZrO₂. From Table 6 we see that the ZrO₂-containing sorbents are generally easier to reduce than pure CeO₂, and that there is relatively little difference in the reducibility of the two sorbents containing 20% and 30% ZrO₂. Comparison of the reduction results in Tables 5 and 6 shows that the LSU sorbents possess intermediate reducibility. Of the ZrO₂-free sorbents, Ce(RP) was most easily reduced, followed by Ce(LSU), and then the Ce(Alfa) and CeC(Alfa). CZ(Nex) sorbents were more easily reduced than those from LSU, but the CZ(LSU) sorbents were somewhat more easily reduced than Ce(RP).

Table 5. Summary of Reduction Results from Commercial Sorbents

Samples	Temperature, °C, Corresponding to Indicated Value of n			Value of n	
	1.98	1.86	1.80	700°C	1000°C
Gas 1					
Ce(RP)	660	840	---	1.97	1.81
Ce(Alfa)	670	850	1000	1.97	1.80
CeC(Alfa)	700	880	---	1.98	1.82
CZ(Nex)85	280	720	840	1.87	1.74
CZ(Nex)80	380	720	820	1.87	1.75
CZ(Nex)70	330	600	740	1.81	1.74
Gas 2					
Ce(RP)	730	---	---	2.00	1.88
Ce(Alfa)	830	---	---	2.00	1.91
CeC(Alfa)	860	---	---	2.00	1.91
CZ(Nex)85	350	860	---	1.91	1.82
CZ(Nex)80	430	850	---	1.91	1.81
CZ(Nex)70	330	670	850	1.85	1.77
Gas 3					
Ce(RP)	730	930	---	1.99	1.85
Ce(Alfa)	770	950	---	1.99	1.85
CeC(Alfa)	765	---	---	2.00	1.87
CZ(Nex)85	320	760	890	1.89	1.77
CZ(Nex)80	280	770	880	1.89	1.77
CZ(Nex)70	330	680	860	1.85	1.76

6. FIXED-BED DESULFURIZATION RESULTS

All test sorbents were first pressed into tablets using a hydraulic press at 20,000 psi. The resulting tablets were crushed and sieved with the 150-300 μm size range used in reaction tests. Sorbent of the desired particle size range was mixed with Al_2O_3 in a 2-to-1 ratio by weight, and a selected amount of the mixture was added to the reactor. Tablets were formed because the small particle size of the as-received sorbent materials produced excessive pressure drop through the reactor, and the Al_2O_3 was added to control sintering. Zeng et al. (1999) found that the sorbent without Al_2O_3 sintered into a loosely bound chalk-like mass during reaction. With the added Al_2O_3 the mixture could be removed from the reactor as a free-flowing powder after tests.

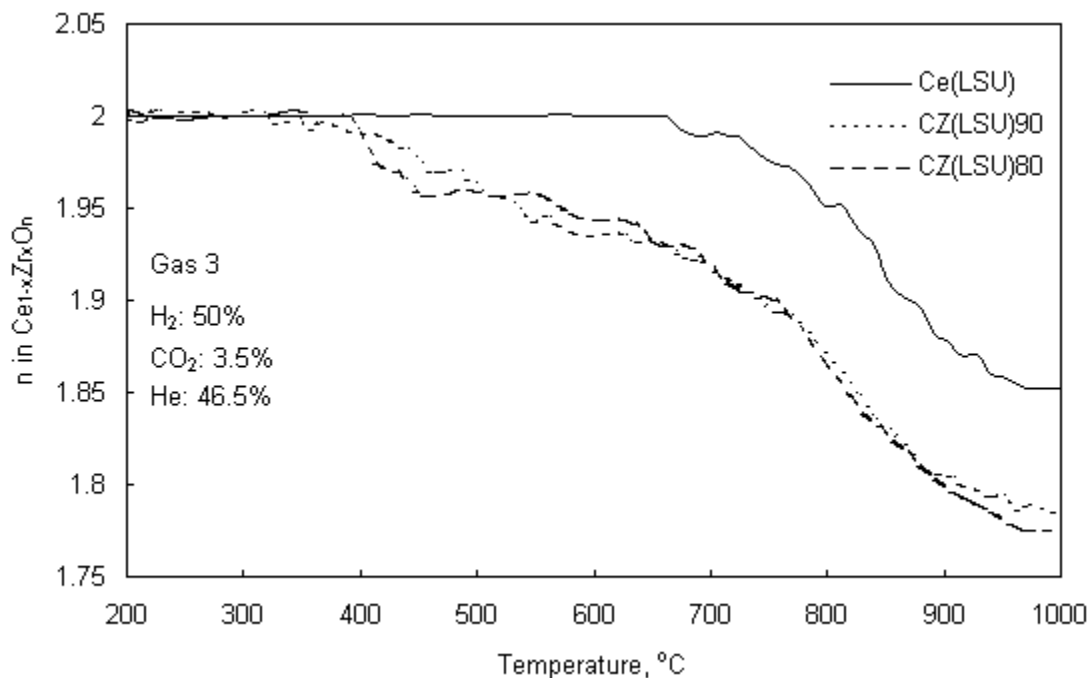


Figure 17. Comparison of Reducibility of Ce(LSU) and CZ(LSU) Sorbents in Gas 3.

Table 6. Summary of Reduction Results for LSU Sorbents

Samples	Temperature, °C, Corresponding to Indicated Value of n			Value of n	
	1.98	1.86	1.80	700°C	1000°C
Gas 1					
Ce(LSU)	630	880	1000	1.97	1.82
CZ(LSU)90	590	850	---	1.95	1.81
CZ(LSU)80	500	800	---	1.94	1.82
Gas 2					
Ce(LSU)	760	---	---	1.99	1.90
CZ(LSU)90	580	960	---	1.95	1.85
CZ(LSU)80	410	950	---	1.95	1.85
Gas 3					
Ce(LSU)	740	940	---	1.99	1.85
CZ(LSU)90	440	810	890	1.92	1.78
CZ(LSU)80	410	800	900	1.91	1.77

Typical breakthrough curves showing H_2S concentration as a function of dimensionless time for two duplicate tests are presented in Figures 18 and 19. Figure 18

illustrates the complete breakthrough curves while Figure 19 shows the results on an expanded concentration scale to emphasize the prebreakthrough region. Dimensionless time is defined as the ratio of the actual reaction time to the time corresponding to complete conversion of CeO_2 to $\text{Ce}_2\text{O}_3\text{S}$ if 100% of the H_2S fed were removed. The dimensionless times are adjusted to account for the loss of volatile material during the initial heating period as well as the different sorbent compositions. The dimensional times in minutes corresponding to dimensionless times of 1.0 and based on 6 g of sorbent with a total sulfidation gas feed rate of $400 \text{ cm}^3(\text{stp})/\text{min}$ containing 0.5mol % H_2S are presented in Table 7.

Figure 18 also shows fractional sorbent conversion as a function of dimensionless time. Sorbent conversion was calculated by numerically integrating the area between the feed H_2S concentration and the H_2S breakthrough curve. For practical purposes during the early stages of the reaction when H_2S removal was almost complete, dimensionless time is also equal to the fractional sorbent conversion. These runs used 6 g of Rhone Poulenc CeO_2 and 3 g of alumina at a total feed rate of $400 \text{ cm}^3(\text{stp})/\text{min}$. Reaction temperature was 800°C and the feed gas contained 49.75% N_2 , 50% H_2 , and 0.5% H_2S . One test was carried out to completion while the second was stopped when the H_2S concentration in the product gas reached 2000 ppmv. On the scale of Figure 18 the results of the two tests are effectively equal; Figure 19 shows only small differences in H_2S concentration during prebreakthrough.

H_2S removal appears to be complete on the concentration scale of Figure 18 up to a dimensionless time of about 0.8. However, Figure 19 shows small concentration

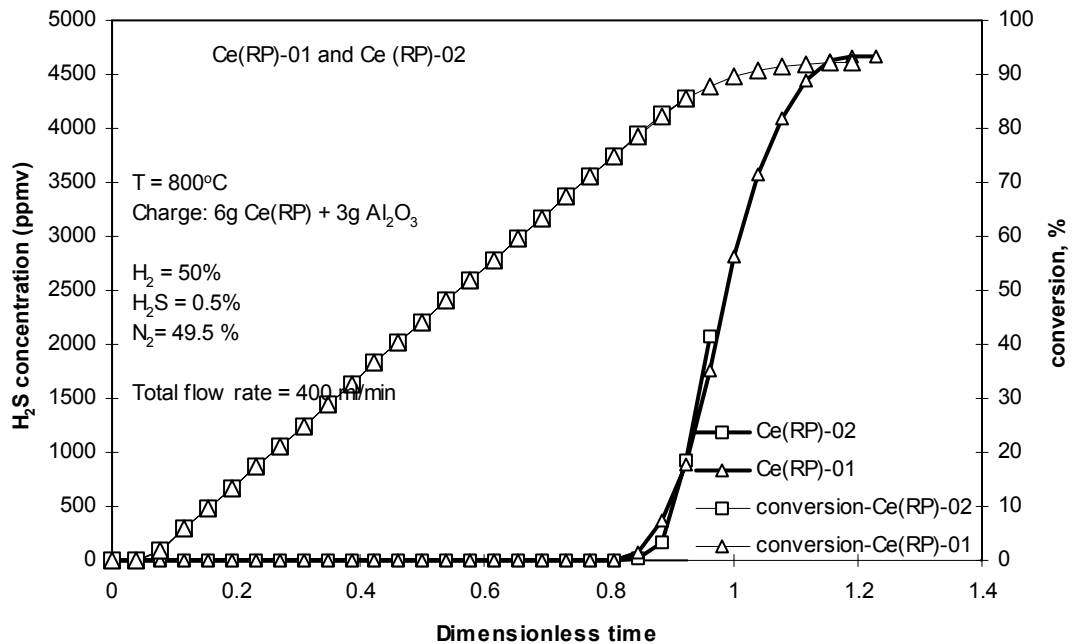


Figure 18. Typical Sulfidation Breakthrough Curves and Sorbent Conversions for Duplicate Tests (Full Concentration Scale).

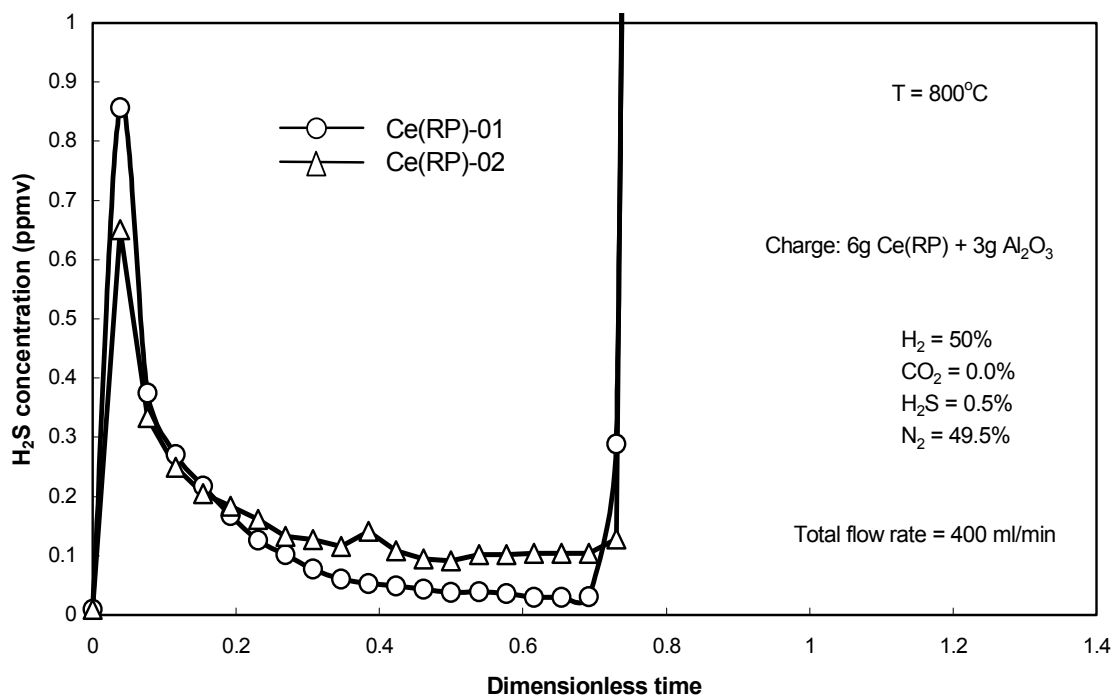


Figure 19. Typical Sulfidation Prebreakthrough Curves for Duplicate Tests (Expanded Concentration Scale).

Table 7. The Relation Between Dimensional Time and Dimensionless Time = 1.0 (see explanation in text)

Sorbent Designation	Time, min
Ce(RP)	179
Ce(Alfa)	184
CeC(Alfa)	151
CZ(Nex)85	191
CZ(Nex)80	196
CZ(Nex)70	203
Ce(LSU)	202
CZ(LSU)90	197
CZ(LSU)80	215

maxima near the beginning of the reaction followed by decreases to approximately 0.1 ppmv H_2S during prebreakthrough. The H_2S concentration began to increase rapidly and exceeded 1 ppmv at dimensionless time just less than 0.8. We attribute the small “bumps” near the beginning of the reaction to the fact that H_2S initially contacted unreduced or partially reduced CeO_2 . However, a reduction reaction front downstream of the sulfidation reaction front soon produced CeO_n with n approaching the equilibrium value in the reducing gas composition. Fractional sorbent conversion was approximately

0.75 at the beginning of active breakthrough and near 0.9 when the postbreakthrough period was reached.

The prebreakthrough region is of primary interest since this region establishes the ultimate H_2S removal potential at the specific reaction conditions. Consequently, most of the experimental results presented in the following sections use an expanded concentration scale comparable to Figure 19.

6.1. Commercial Sorbents

Figure 20 compares the prebreakthrough results from three commercial ceria sorbents (no ZrO_2). Reaction conditions are given on the figure. Overall sulfidation profiles (comparable to Figure 18) were quite similar. However, in the expanded concentration scale differences are clearly evident. Both CeC(Alfa) and Ce(RP) successfully reduced the H_2S concentration to below 1 ppmv for extended time periods. The prebreakthrough period lasted to a dimensionless time just over 0.7 using Ce(RP) but was just less than 0.6 with CeC(Alfa) . In contrast the minimum H_2S concentration achieved with Ce(Alfa) sorbent was about 6 ppmv and there was no true prebreakthrough period in which the concentration was below 1 ppmv. The results of these tests were qualitatively consistent with the reduction and characterization tests. Ce(RP) showed the greatest level of reduction while CeC(Alfa) and Ce(Alfa) showed similar reductions levels. XRD analysis showed that Ce(Alfa) had the largest crystal size among the three. Because the performance of Ce(RP) was consistently superior to that of the other Ce sorbents, it was used in most of the tests of commercial ZrO_2 -free CeO_2 sorbents.

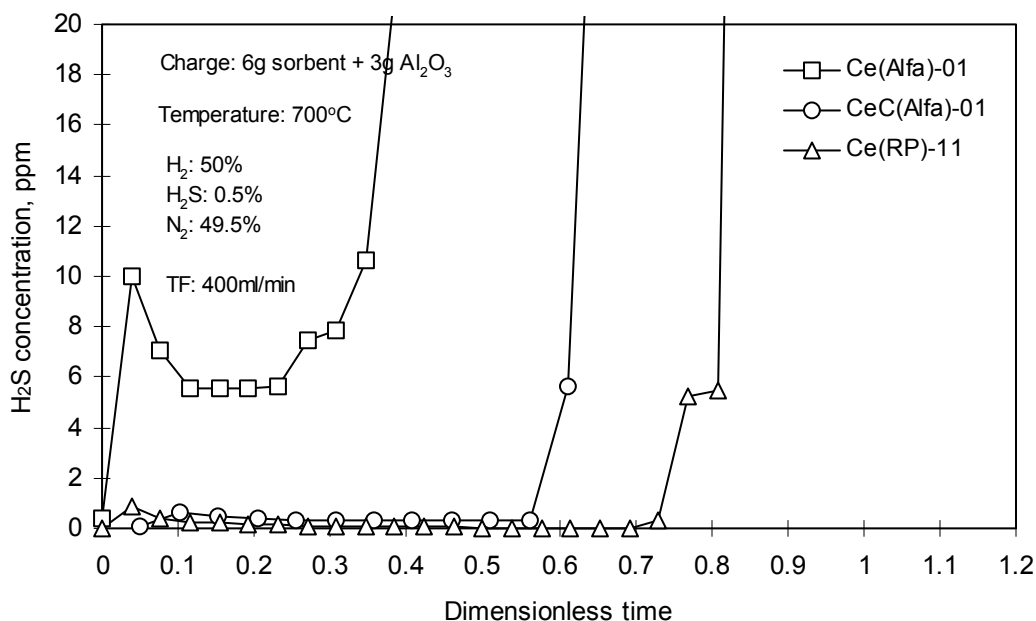


Figure 20. Prebreakthrough Sulfidation Results from Three Commercial CeO_2 Sorbents

The effect of temperature on H_2S capture using sorbent Ce(RP) during the prebreakthrough region is shown in Figure 21. Other reaction conditions are shown on

the figure. H_2S concentration was below 1 ppmv for extended time periods at all three temperatures. Each test showed the small initial H_2S maximum, which we attribute to incomplete reduction during the early stages of the test. The magnitude of the maximum decreased from about 3 ppmv at 800°C to 1 ppmv at 700°C to less than 0.5 ppmv at 600°C . In addition, at a dimensionless time of 0.5, the 800°C test produced the highest H_2S concentration of 0.5 ppmv, compared to about 0.1 ppmv H_2S at the two lower temperatures. However, the duration of the prebreakthrough period decreased as temperature decreased, from a maximum of 0.82 at 800°C to a minimum of 0.58 at 600°C .

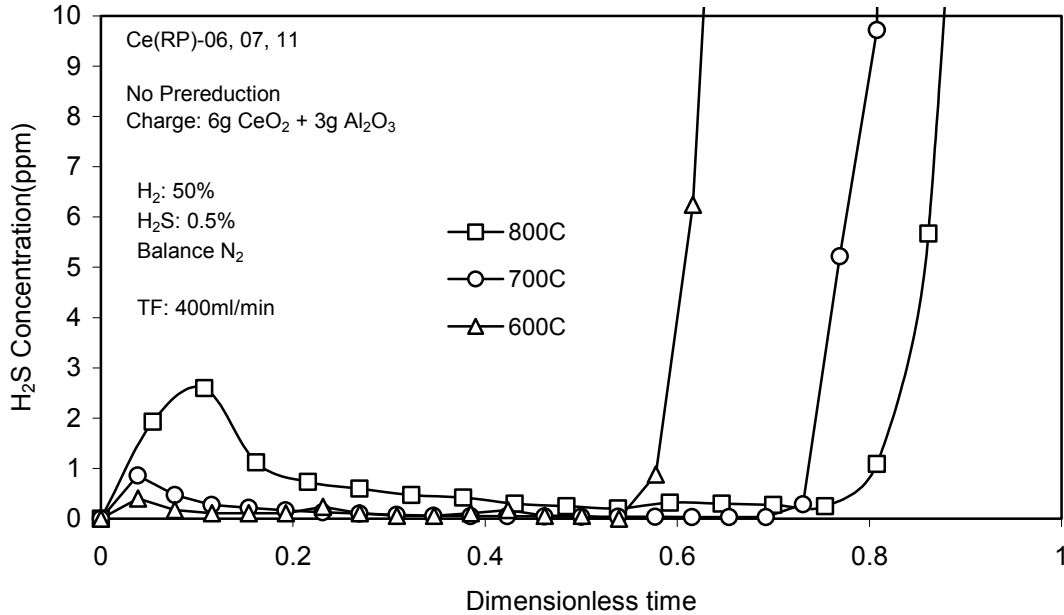


Figure 21. The Effect of Temperature on the Sulfidation of Ce(RP)

Figure 22 compares the sulfidation performance of Ce(RP) with two sorbents from NexTech, CZ(Nex)85 and CZ(Nex)80. Although all three sorbents were successful in reducing the H_2S concentration to below 1 ppmv for extended time periods, the results were unexpected since both the prebreakthrough H_2S concentration and, in particular, the duration of the prebreakthrough period were superior with Ce(RP). The performance of the CZ sorbents was quite similar, although the prebreakthrough H_2S concentration was marginally lower at the higher ZrO_2 level.

While these tests suggested that ZrO_2 addition actually had a negative effect on desulfurization performance, it is important to recognize that Ce(RP) and CZ(Nex) were supplied by different manufacturers, prepared using different methods, and possessed different structural properties. The crystal size of the Ce(RP) sorbent was considerably smaller than the CZ(Nex) crystal sizes, while the surface area was considerably larger. These more favorable physical properties might overwhelm the effect of ZrO_2 addition. For example, if CZ(Nex) performance was compared to Ce(Alfa) performance, we would conclude that ZrO_2 addition had a positive effect on performance, a conclusion that might also be false since the properties of CZ(Nex) are superior to those of Ce(Alfa).

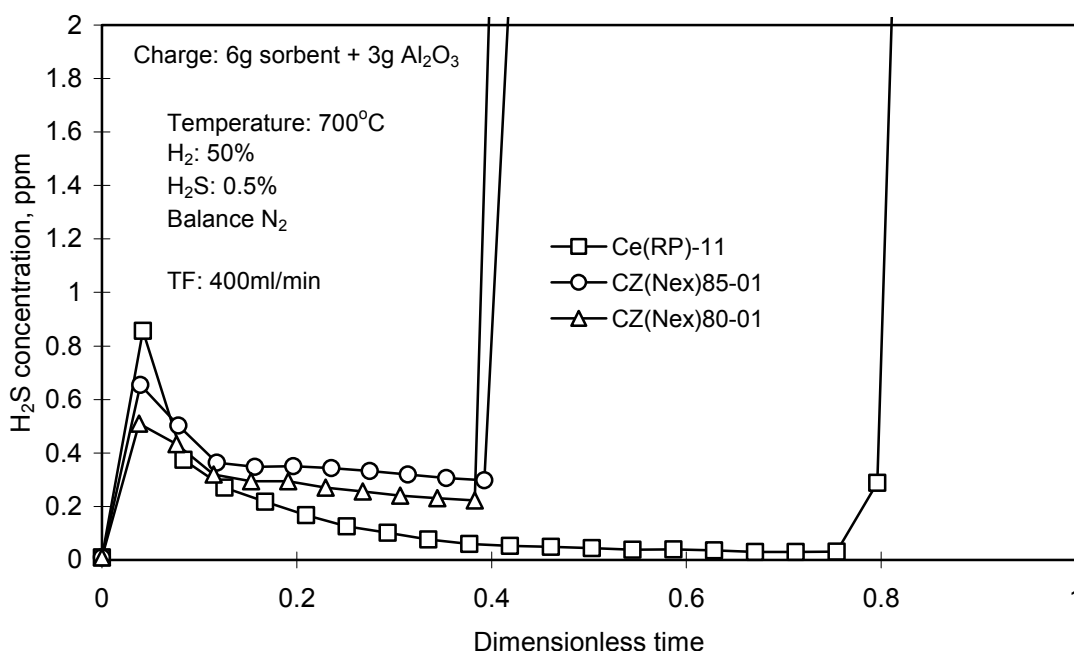


Figure 22. Comparison of the Sulfidation Performance of Ce(RP) and CZ(Nex)

These results led us to conclude that sorbents having similar chemical and physical properties would be required to fairly evaluate the effect of ZrO_2 addition, and led to the in-house preparation and study of LSU sorbents. These results are described in the next section of this report.

6.2. LSU Sorbents

Three sorbents -- Ce(LSU), CZ(LSU)90, and CZ(LSU)80 -- were prepared in-house using the precipitation and co-precipitation techniques previously described. Properties of these sorbents were reasonably similar and the sorbents were used to evaluate the effect of ZrO_2 addition.

Reaction conditions were changed from those described in the previous section. Sorbent charge was reduced from 6 g to 2 g, total gas feed rate was reduced from 400 sccm to 80 sccm, and the H_2S content of the feed gas was reduced from 0.5 mol% to 0.25 mol%. The reduction in sorbent charge was made to conserve sorbent, while the feed rate and composition changes were made to offset the reduction in sorbent and provide sufficient reaction time so that the prebreakthrough, breakthrough, and postbreakthrough periods were clearly visible. At these conditions the dimensional times corresponding to dimensionless time = 1.0 are 674 min, 658 min, and 716 min for Ce(LSU), CZ(LSU)90, and CZ(LSU)80, respectively.

Figure 23 compares the prebreakthrough performance of the three sorbents. Sulfidation was at 700°C in a highly reducing gas containing 0.25% H_2S , 10% H_2 , and 89.75% N_2 flowing at 80 cm^3 (STP)/min. Prebreakthrough H_2S concentrations were near

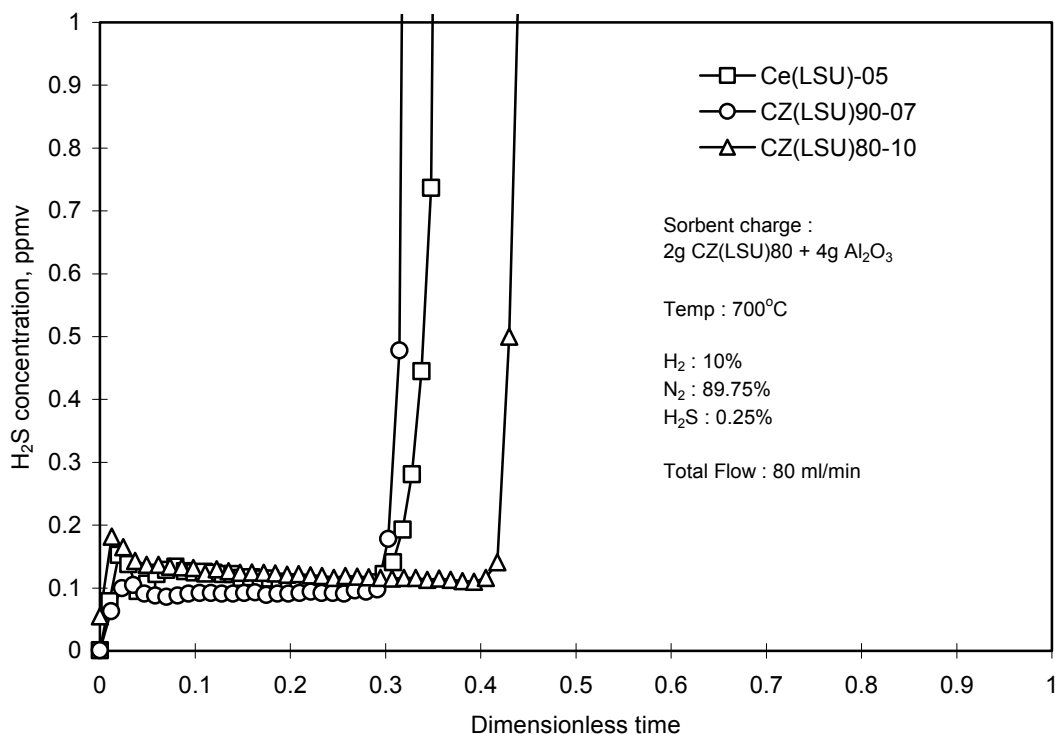


Figure 23. Comparison of Sulfidation Performance on Ce(LSU), CZ(LSU)90, and CZ(LSU)80

0.1 ppmv for all three sorbents, but the duration of the prebreakthrough period using Ce(LSU) was somewhat longer.

In one series of tests the sorbents were pre-reduced for 4 hours using the same gas composition (except for H₂S) and temperature as used in the subsequent sulfidation test. Example results are presented in Figure 24 for sorbent CZ(LSU)80; the effect was similar for the other LSU sorbents. Pre-reduction reduced the prebreakthrough H₂S concentration from 0.1 – 0.2 ppmv to near zero, and extended the duration of the prebreakthrough period from a dimensionless time of about 0.4 to 0.5.

The effect of temperature on the sulfidation performance of CZ(LSU)80, shown in Figure 25, was qualitatively similar to that of CE(RP) sorbent shown in Figure 21. As the sulfidation temperature decreased, both the prebreakthrough H₂S concentration and the duration of the prebreakthrough period decreased. Even at the maximum temperature of 750°C the prebreakthrough concentration was less than about 0.2 ppmv, while at the two lower temperatures the prebreakthrough concentration was about 0.1 ppmv. However, the prebreakthrough time at 750°C was about 3 times greater than at 600°C.

The addition of CO₂ decreases the reducing power of the sulfidation gas and also the ability of the sorbent to remove H₂S. This effect is shown in Figures 26 and 27 for sorbent Ce(LSU). Figure 26 shows the full sulfidation breakthrough curve while Figure

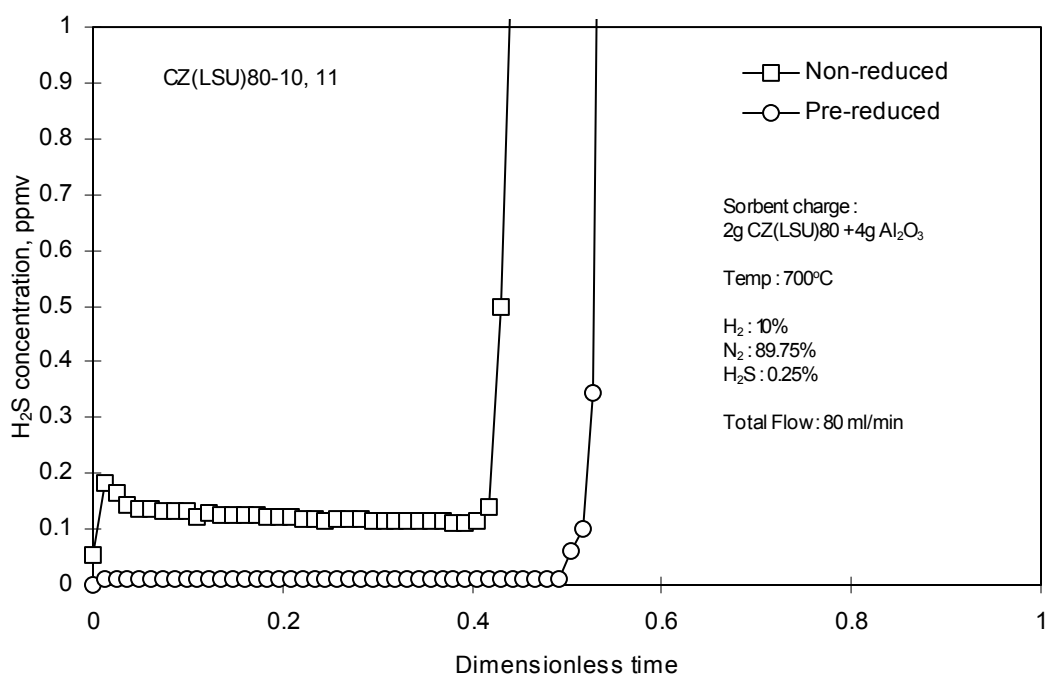


Figure 24. The Effect of Pre-Reduction of Sulfidation on CZ(LSU)80

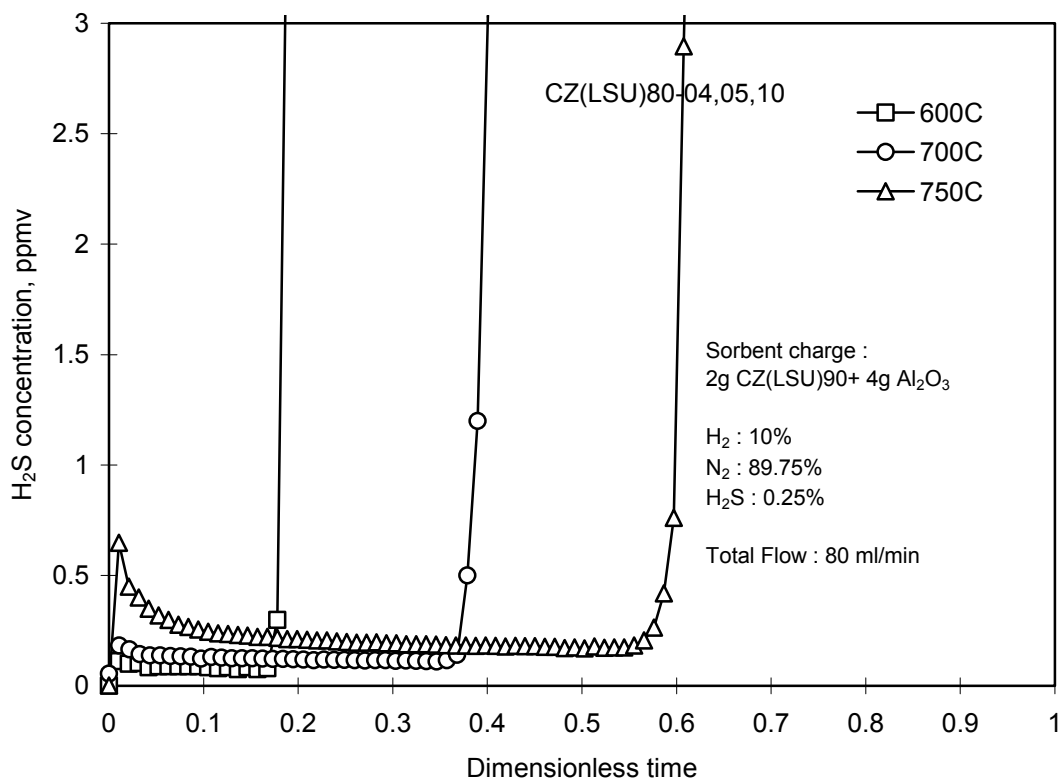


Figure 25. The Effect of Temperature on Sulfidation of CZ(LSU)80

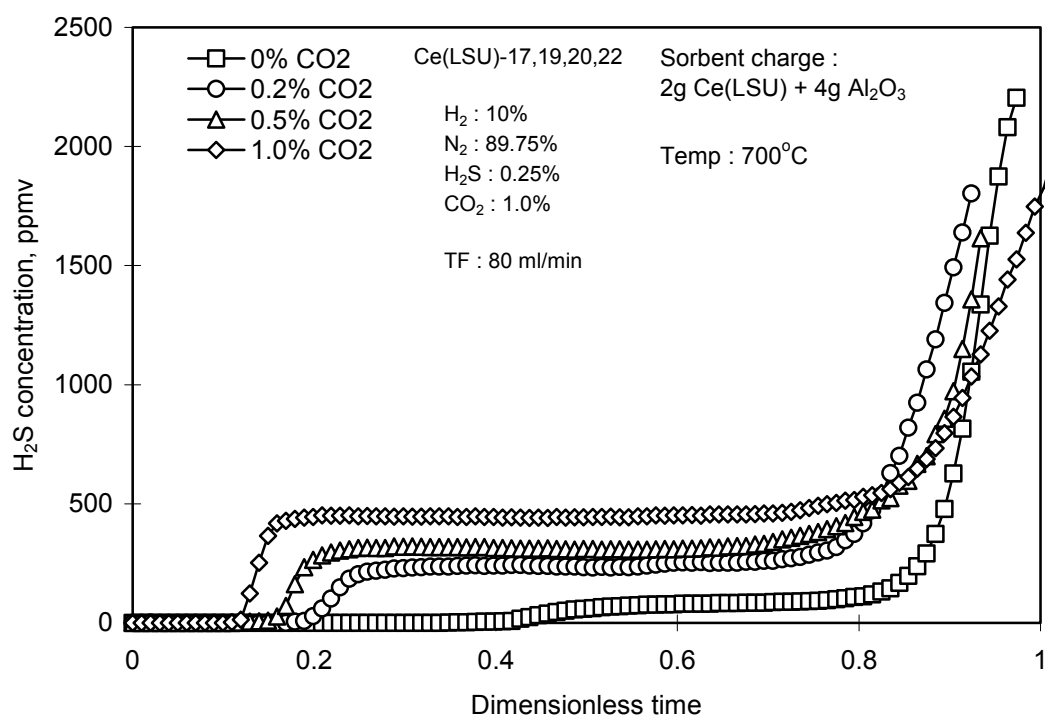


Figure 26. The Effect of CO₂ in the Sulfidation Gas on Performance of Ce(LSU) (Full Concentration Scale).

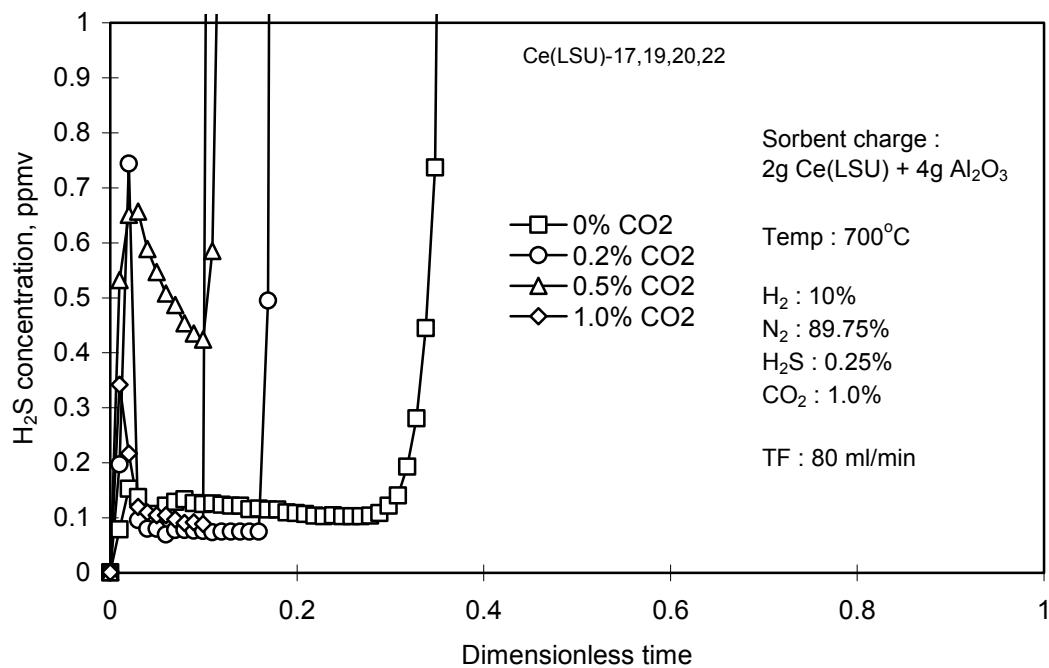


Figure 27. The Effect of CO₂ in the Sulfidation Gas on Performance of Ce(LSU) (Expanded Concentration Scale).

27 emphasizes the prebreakthrough region using an expanded H₂S concentration scale. The existence of two steady-state periods prior to final breakthrough is clearly evident in Figure 27. During the initial prebreakthrough period, shown more clearly in Figure 27, the H₂S concentration was below 1 ppmv even with 1% CO₂ in the sulfidation feed gas. However, the duration of this prebreakthrough period decreased as the CO₂ concentration increased. The onset of the second steady state or plateau region in Figure 27 occurred at earlier dimensionless times as the CO₂ concentration increased; the H₂S concentration during the plateau also increased with increasing CO₂ concentration. However, final breakthrough occurred at roughly the same dimensionless time in all four cases.

A somewhat similar effect was observed using CZ(LSU)80 when CO₂ was added to the sulfidation feed gas as shown in Figures 28 (full concentration scale) and 29 (expanded concentration). Once again H₂S concentration during the first prebreakthrough period was less than 1 ppmv and the duration of this period decreased as the CO₂ concentration increased. However, there was no true plateau region. At the end of prebreakthrough there was a rapid increase in H₂S concentration followed by an extended period in which the slopes of the H₂S-dimensionless time curves decreased but

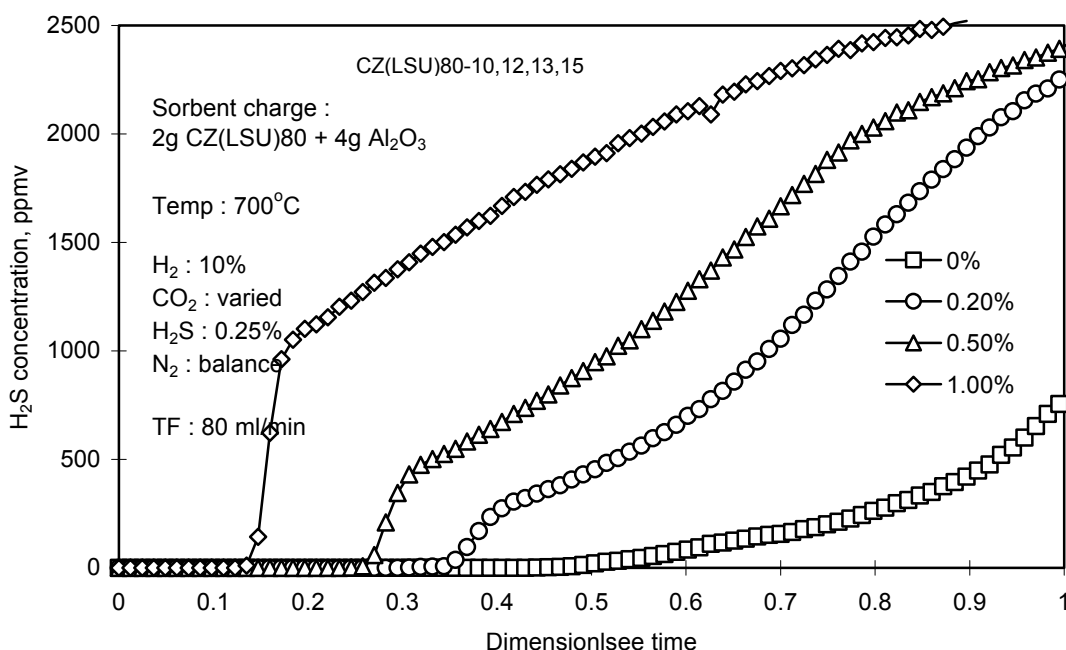


Figure 28. The Effect of CO₂ in the Sulfidation Gas on Performance of CZ(LSU)80 (Full Concentration Scale).

7. CONCLUSIONS

The electrochemical production of CeO₂-ZrO₂ powders with nanometric crystallites has been demonstrated for the first time. The XRD and TEM properties of the electrosynthesized CeO₂-ZrO₂ confirmed the existence of a solid solution of ZrO₂ in

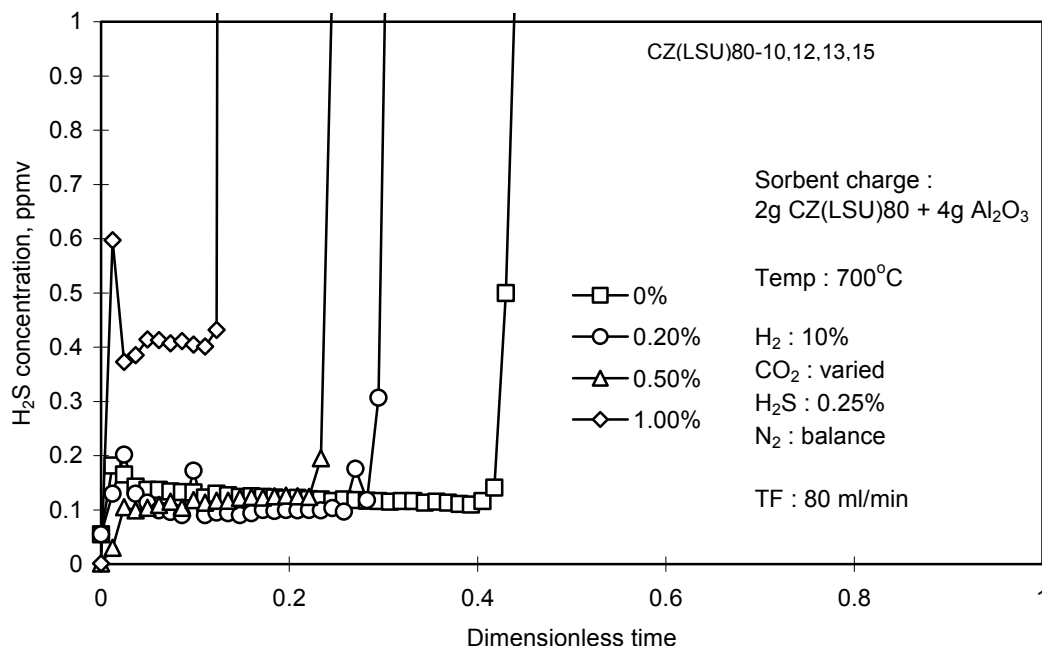


Figure 29. The Effect of CO₂ in the Sulfidation gas on Performance of CZ(LSU)80 (Expanded Concentration Scale).

CeO₂ were measured at Ce to Zr ratios of interest. A separate ZrO₂ phase could be identified only at quite high concentrations of ZrO₂. Unfortunately, the quantities of sorbent produced electrochemically were not sufficient to carry out a desulfurization test program. Hence, CeO₂ and CeO₂-ZrO₂ materials from a number of other sources were considered.

A laboratory-scale, fixed-bed, atmospheric-pressure reactor system was constructed to carry out the desulfurization experiments. All parts of the system that contacted low concentrations of H₂S were constructed of quartz, Teflon, or silcosteel to prevent interaction with the H₂S. Product gas analysis was accomplished using a Varian Model 3800 gas chromatograph equipped with a pulsed flame photometric detector (PFPD) capable of detecting H₂S to approximately 0.1 ppmv.

Six CeO₂ and CeO₂-ZrO₂ sorbents were obtained from commercial sources for desulfurization testing. In addition to desulfurization screening tests, these sorbents were subjected to x-ray diffraction analysis, their BET surface area was determined both in the as-received state and following high temperature calcination, and their reducibility was measured as a function of temperature and reducing gas composition. Five of the six commercial sorbents tested were capable of removing H₂S to less than 1 ppmv when a highly reducing feed gas composition was used. However, because of the limited quantities of sorbents available and the differing properties, it proved to be impossible to evaluate the effect of ZrO₂ addition.

As a result, one CeO₂ and two CeO₂-ZrO₂ sorbents were synthesized in-house using a co-precipitation technique. Characterization and testing of these sorbents was emphasized during year 03 of the project. XRD analysis showed that the added ZrO₂ formed a solid solution in CeO₂. Structural properties of the three sorbents were reasonably constant. The desulfurization ability of these sorbents was studied as a function of temperature, reducing strength of the feed gas, and pre-reduction in a H₂S-free gas prior to sulfidation. All sorbents were capable of reducing the H₂S concentration from 2500 ppmv in the feed gas to less than 1 ppmv in the product gas. Pre-reduced sorbents were capable of reducing the H₂S concentration to below the 0.1 ppmv detection limit of the PFPD for extended time periods.

8. REFERENCES

- Bevan, D. and Kordis, J., 1964, Mixed Oxides of the Type MoO₃ – 1. Oxygen Dissociation Pressure and Phase Relationship in the System CeO₂-Ce₂O₃ at High Temperatures, *Journal of Inorganic and Nuclear Chemistry*, 26, 1509.
- Bunluesin, T., Gorte, R., and Graham, G., 1997, CO Oxidation for the Characterization of Reproducibility in Oxygen Storage Components of Three-Way Automotive Catalysts, *Applied Catalysis B., Environmental*, 14, 105.
- Colon, G., Pijolat, M., Valdivieso, F., Vidal, H., Kaspar, J., Daturi, M., Binet, C., Lavelley, J., Baker, R., and Bernal, S., 1998, Surface and Structural Characterization of Ce_xZr_{1-x}O₂ mixed Oxides as Potential Three-Way Catalyst Promoters, *Journal of the Chemical Society, Faraday Transactions*, 94, 3717.
- Cuif, J.-P., Blanchard, G., Touret, O., Marczi, M., and Quemere, E., 1996, Proceedings of the 1996 International Fall Fuels and Lubricants Meeting of the Society of Automotive Engineers, San Antonio, TX, 73.
- Focht, G. D., Ranade, P. V., and Harrison, D. P., 1988, High Temperature Desulfurization Using Zinc Ferrite: Reduction and Sulfidation Kinetics, *Chemical Engineering Science*, 43, 3005.
- Gibson, J. B., and Harrison, D. P., 1980, The Reaction Between Hydrogen Sulfide and Single Spherical Pellets of Zinc Oxide, *Industrial and Engineering Chemistry, Process Design and Development*, 19, 231.
- Harrison, D. P., 1998, Performance Analysis of ZnO-Based Sorbents in Removal of H₂S from Fuel Gas, in *Desulfurization of Hot Coal gas*, A. Atimtay and D. P. Harrison, eds., Springer, Berlin, 213.
- Hori, C., Permana, H., Ng, K., Brenner, A., Moore, K., Rahmoeller, K., and Belton, D., 1998, Thermal Stability of Oxygen Storage Properties in a Mixed CeO₂-ZrO₂ System, *Applied Catalysis B, Environmental*, 16, 105.

Mukherjee, A., Yi, K., Podlaha, E., and Harrison, 2001, High Efficiency Desulfurization of Synthesis Gas, Annual Report, U.S Department of Energy Project DE-PS26-00FT40676.

Ozawa, M., 1997, Role of Cerium-Zirconium Mixed Oxides as Catalysts for Car Pollution: A Short Review, Journal of Alloys and Compounds, 275, 886.

Podlaha, E. P., Bogli, A., Bonhote, Ch., and Landolt, D., 1997, Development of a New, Pseudo-Inverted Disk Electrode, Journal of Applied Electrochemistry, 27, 805.

Rossignol, S., et al., 1999, Preparation of Zirconia-Ceria Materials by Soft Chemistry, Catalysis Today, 50, 261.

Sorensen, O., 1976, Thermodynamic Studies of the Phase Relationships of Nonstoichiometric Cerium Oxides at Higher Temperatures, Journal of Solid State Chemistry, 18, 217.

Switzer, A., 1987, Electrochemical Synthesis of Ceramic Films and Powders, Journal of the American Ceramic Society Bulletin, 66[10], 1521.

Trovarelli, A., 1996, Catalytic Properties of Ceria and CeO₂-Containing Materials, Catalysis Reviews: Science and Engineering, 38, 439.

Trovarelli, A., de Leitenburg, C., and Colcetti, G., 1997, Design Better Cerium-Based Oxidation Catalysts, CHEMTECH, 27, 32.

Woods, M. C., Gangwal, S. K., Jothimurugesan, K., and Harrison, D. P., 1990, The Reaction Between H₂S and Zinc Oxide-Titanium Oxide Sorbent: 1. Single Pellet Kinetic Studies, Industrial and Engineering Chemistry Research, 29, 1160.

Yi, K., Podlaha, E., and Harrison, 2002, High Efficiency Desulfurization of Synthesis Gas, Annual Report, U.S Department of Energy Project DE-PS26-00FT40676.

Zamar, F., Travarelli, A., de Leitenburg, C., and Dolcetti, G., 1995, CeO₂-Based Solid Solutions with the Fluorite Structure as Novel and Effective Catalysts for Methane Combustion, Journal of the Chemical Society, Chemical Communications, 965.

Zeng, Y, Zhang, S., Groves, F. R., and Harrison, D. P., 1999, High Temperature Gas Desulfurization with Elemental Sulfur Production, Chemical Engineering Science, 54, 3007.

Zeng, Y., 1999a, Cerium Oxide as a Highly Effective and Durable High Temperature Desulfurization Sorbent, Ph. D. Dissertation, Louisiana State University.

Zeng, Y., Kaytakoglu, S., and Harrison, D. P., 2000, Reduced Cerium Oxide as an Efficient and Durable High Temperature Desulfurization Sorbent, *Chemical Engineering Science*, 55, 4893.

Zhou, Y., Phillips, R. J., and Switzer, J., 1995, Electrochemical Synthesis and Sintering of Nanocrystalline Cerium(IV) Oxide Powders, *Journal of the American Ceramic Society*, 78, 981.